PCCP

PAPER

View Article Online
View Journal | View Issue

Cite this: *Phys. Chem. Chem. Phys.*, 2017, **19**, 13049

Assessment of electronic structure methods for the determination of the ground spin states of Fe(II), Fe(III) and Fe(IV) complexes†

Pragya Verma, *[abc] Zoltan Varga,[ab] Johannes E. M. N. Klein,[ad] Christopher J. Cramer,[abc] Lawrence Que Jr.[ad] and Donald G. Truhlar *[abc]

Received 26th February 2017,
Accepted 27th April 2017

DOI: 10.1039/c7cp01263b

rsc.li/pccp

Our ability to understand and simulate the reactions catalyzed by iron depends strongly on our ability to predict the relative energetics of spin states. In this work, we studied the electronic structures of Fe^{2+} ion, gaseous FeO and 14 iron complexes using Kohn–Sham density functional theory with particular focus on determining the ground spin state of these species as well as the magnitudes of relevant spin-state energy splittings. The 14 iron complexes investigated in this work have hexacoordinate geometries of which seven are Fe(II), five are Fe(III) and two are Fe(IV) complexes. These are calculated using 20 exchange–correlation functionals. In particular, we use a local spin density approximation (LSDA) – GVWN5, four generalized gradient approximations (GGAs) – BLYP, PBE, OPBE and OLYP, two non-separable gradient approximations (NGAs) – GAM and N12, two meta-GGAs – M06-L and M11-L, a meta-NGA – MN15-L, five hybrid GGAs – B3LYP, B3LYP*, PBE0, B97-3 and SOGGA11-X, four hybrid meta-GGAs – M06, PW6B95, MPW1B95 and M08-SO and a hybrid meta-NGA – MN15. The density functional results are compared to reference data, which include experimental results as well as the results of diffusion Monte Carlo (DMC) calculations and ligand field theory estimates from the literature. For the Fe^{2+} ion, all functionals except M11-L correctly predict the ground spin state to be quintet. However, quantitatively, most of the functionals are not close to the experimentally determined spin-state splitting energies. For FeO all functionals predict quintet to be the ground spin state. For the 14 iron complexes, the hybrid functionals B3LYP, MPW1B95 and MN15 correctly predict the ground spin state of 13 out of 14 complexes and PW6B95 gets all the 14 complexes right. The local functionals, OPBE, OLYP and M06-L, predict the correct ground spin state for 12 out of 14 complexes. Two of the tested functionals are not recommended to be used for this type of study, in particular M08-SO and M11-L, because M08-SO systematically overstabilizes the high spin state, and M11-L systematically overstabilizes the low spin state.

1 Introduction

The mechanisms of reactions catalyzed by iron depend strongly on the spin state,[1,2] and our ability to understand and simulate these reactions depends strongly on our ability to predict the relative energetics of the relevant spin states accurately.[3] Evaluating the spin-state energetics should be very important for understanding exchange-enhanced reactivity.[4–6] Fe(II) and Fe(III) complexes are ubiquitous in nature and can be found in a number of biological systems and as catalysts for a number of important chemical and biological reactions.[7,8] Iron-containing metal–organic frameworks (MOFs) and zeolites in many instances have interesting catalytic properties,[9,10] and iron is also a convenient metal for use in the templated self-assembly of metal–organic cages.[11–13]

Of particular interest are the activation of dioxygen mediated by iron complexes in these oxidation states[14–17] and the temperature-dependent transition from a low-spin state to a high-spin state ("spin crossover") for hexacoordinate iron complexes.[18–20] The higher oxidation states (IV, V and VI) of iron also exist or are

[a] *Department of Chemistry, University of Minnesota, Minneapolis, Minnesota 55455-0431, USA. E-mail: verma045@umn.edu, truhlar@umn.edu*
[b] *Chemical Theory Center and Minnesota Supercomputing Institute, University of Minnesota, Minneapolis, Minnesota 55455-0431, USA*
[c] *Nanoporous Materials Genome Center, University of Minnesota, Minneapolis, Minnesota 55455-0431, USA*
[d] *Center for Metals in Biocatalysis, University of Minnesota, Minneapolis, Minnesota 55455-0431, USA*

† Electronic supplementary information (ESI) available: Details of conversion of r_0 to r_e, relative energies of conformers of complexes **13** and **14**, figure showing the conformers of complexes **13** and **14**, $\langle S^2 \rangle$ values of Fe^{2+} ion, FeO and the **14** complexes and coordinates of PW6B95/def2-TZVP and M06-L/def2-TZVP optimized geometries of all the **14** complexes. See DOI: 10.1039/c7cp01263b

proposed to exist and are implicated in reactions such as C–H and C–C bond activation.[9,21–26] The Fe(II) and Fe(III) oxidation states are the more commonly occurring oxidation states in many extended systems, such as iron-based MOFs[27–30] and iron-containing zeolites.[31–33] The kind of chemistry exhibited by these extended systems is governed by the nature of the ground spin state for a single-state reactivity scenario, whereas in a two-state reactivity scenario, crossing of spin surfaces can occur during the course of a reaction leading to spin inversion, which can play an important role in determining the rate of the reaction.[34,35] As such, the accurate prediction of the structures and energies of the ground and excited spin states is a crucial step toward understanding iron-catalyzed reactions.

It is essential to understand how well various electronic structure methods perform in determining the ground spin state of small or model systems before one applies these methods to study the reactivity of open-shell biological systems and extended materials such as iron-containing MOFs and zeolites. Many papers show the success and failure of different exchange–correlation functionals, dating back at least to the work of Trautwein and coworkers.[36] A review by Kepp[37] reported on the influence of zero-point enthalpy, entropy, free energy, solvation, relativity and dispersion energy on the spin state splittings. In the present work, we study the electronic structures of Fe^{2+} ion, gaseous FeO and 14 iron complexes, each of which has six ligands coordinated to the metal center. Theoretical calculations using Kohn–Sham density functional theory (KS-DFT) for some of these complexes have been reported in the literature by several groups,[37–48] and the present work extends those studies by including more complexes and newer density functionals.

The accuracy of predictions made by KS–DFT depends strongly on the exchange–correlation functional, and this is especially true for predicting the ground spin state of open-shell systems containing transition metals. The choice of a functional for practical studies of a given system and a given property is made in part on the basis of previous validations and also on the basis of the functional's ingredients, which in practice influence its accuracy and computational cost. Local functionals (which are functionals without Hartree–Fock (HF) exchange and without nonlocal correlation) have relatively low computational cost, but they suffer from self-interaction errors and are known to often overstabilize low-spin states.[49–52] Definitive analysis of this tendency is complicated though by the change in angular shape of the orbitals that may accompany spin changes, which couples errors in exchange energy to errors in describing orbitals of different angular momentum or shape.[53–56] Hybrid functionals substitute a percentage of local exchange by HF exchange, and this eliminates some of the self-interaction error.[57] This improved treatment of self-interaction is achieved at the expense of increased computational costs for large systems, thus limiting the size of the systems that can be studied. Furthermore, hybrid functionals are not necessarily more accurate. Whereas local functionals produce overly delocalized charge distributions, high-HF exchange favors overly localized charge distributions. Computed properties often depend on the amount of HF exchange in a hybrid functional, and spin-state splittings can vary especially significantly with the percentage of HF exchange. As a pertinent example, Reiher *et al.*[58–61] and other workers[40,62] have noted that 15–30% HF exchange is optimum for predicting the relative energy orderings of the high- and low-spin states of some transition metal complexes for the exchange–correlation functionals they studied; however, in other work, good results were obtained[43,45,60,63–65] with the local OPBE,[66,67] OLYP[66,68] and RPBE[69] functionals, although in ref. 70 both hybrid and local functionals were found to predict similar ground-state spins, but with hybrid functionals having a greater tendency to favor high-spin states. In a recent study,[47] B2-PLYP,[71] which is a doubly hybrid functional with 53% HF exchange and 27% nonlocal correlation, was shown to predict spin-state splitting energies well. Although the percentage of HF exchange needed to obtain agreement between experiment and computation varies with the transition metal and the ligand, increasing the percentage too much can overstabilize the high-spin states. Also, HF exchange brings in static correlation error, resulting in unsatisfactory predictions for systems with intrinsically multi-configurational wave functions.[72] Yet another complication is that although high HF percentages favor high-spin states, correlation energy favors low-spin states with more doubly occupied orbitals, so when one compares functionals differing in both exchange and correlation functionals, one cannot easily disentangle the contributions. For this and other reasons (*e.g.*, exchange functionals differ in the dependence of their local part on spin densities, spin density gradients, and sometimes local kinetic energy, as well as differing in the percentage of HF exchange), one must consider the exchange–correlation functional as a whole, and not just the amount of the HF exchange.[73] In the present work, a variety of density functionals including ones recently developed in our group, are examined to learn how well they predict the ground spin state of Fe^{2+} atomic ion, FeO diatomic and 14 polyatomic iron complexes with the iron ion spanning three oxidation states.

Two wave function theory (WFT) approaches that can be used as benchmarks for density functional calculations are diffusion Monte Carlo (DMC)[74,75] and the complete active space second order perturbation theory (CASPT2),[76] although CASPT2 is sensitive to the IPEA shift empirical parameter.[77] Density matrix renormalization group (DMRG) calculations[78] and multiconfiguration pair-density functional theory (MC-PDFT)[79,80] are also efficient and promising methods for spin-state energetics in TM complexes. Droghetti *et al.*[39] previously reported the results of DMC calculations on four Fe(II) complexes. They compared the results obtained with DMC with those obtained with LSDA,[94] BP86,[81,82] B3LYP,[68,81,83,100] PBE0[101] and BHH[83] exchange–correlation functionals. They found that these functionals fail badly in quantitatively predicting the energy differences between the high- and low-spin states of all four studied iron complexes. The failure of these functionals was attributed to either an underestimation of the exchange energy (important for complexes with high-spin ground states) or to the multiconfigurational character of the iron complexes (important for complexes with low-spin ground states). The present work will re-examine this kind of problem by considering more cases and more density functionals. One often finds that local density

functionals stabilize the low-spin state and hybrid density functionals stabilize the high-spin state.[49,51] In this work, we test to see to what extent this is true and whether local functionals (which are less expensive than hybrid functionals) perform as well as hybrid functionals.

Considering CASPT2 as a benchmark level, Pierloot and co-workers have examined this model for iron–heme systems,[84] as well as for various hexacoordinate compounds including three of those considered here.[44,64] In the case of the heme compounds, CASPT2 was found to predict excellent spin state energetics for Fe(III) but to systematically overstabilize the high-spin states of the Fe(II) cases by about 5 kcal mol^{-1}. Still larger overstabilizations were observed with a number of density functionals. In the hexacoordinate compounds, CASPT2 results were found to be accurate when reasonably complete single-particle basis sets were employed, and the generally excellent performance of OLYP was noted. Similarly, Isley *et al.*[65] noted good agreement between CASPT2 and OPBE for various geometries of hexacoordinate Fe(II) pyridyl imine complexes, adding to the number of reports of the OptX exchange functional[66] (which is abbreviated as "O" in OLYP and OPBE) providing good accuracy for iron spin-state energetics.

This work is organized as follows. Section 2 describes the iron complexes investigated in this work, Section 3 describes the computational details of density functional and wave function based methods used in this work, Section 4 discusses the results obtained for the 14 iron complexes, and Section 5 concludes our work.

2 Structures

The 14 hexacoordinate iron complexes investigated in this work are as follows; all 14 are shown in Fig. 1 and 2. Seven of them are Fe(II) complexes—

1, $[Fe(CO)_6]^{2+}$;
2, $[Fe(CNH)_6]^{2+}$;
3, $[Fe(NCH)_6]^{2+}$;
4, $[Fe(NH_3)_6]^{2+}$;
5, $[Fe(H_2O)_6]^{2+}$;
6, $[Fe(bipy)_3]^{2+}$; and
7, $Fe(amp)_2Cl_2$.

Five are Fe(III) complexes—

8, $[Fe(CO)_6]^{3+}$;
9, $[Fe(CNH)_6]^{3+}$;
10, $[Fe(NCH)_6]^{3+}$;
11, $[Fe(NH_3)_6]^{3+}$; and
12, $[Fe([9]aneN_3)_2]^{3+}$.

The last two are Fe(IV) complexes—

13, $[Fe(O)(TMC)(MeCN)]^{2+}$ and
14, $[Fe(O)(TMCS)]^{+}$.

Here, bipy stands for 2,2′-bipyridine, amp stands for 2-(aminomethyl) pyridine, [9]aneN$_3$ stands for 1,4,7-triazacyclononane, TMC stands for 1,4,8,11-tetramethyl-1,4,8,11-tetraazacyclotetradecane and TMCS stands for 1-mercaptoethyl-4,8,11-trimethyl-1,4,8,11-tetraazacyclotetradecane.

For the Fe(II) complexes, the energies of the quintet, triplet and singlet states were computed, and in some cases the septet state was also computed; for the Fe(III) complexes, the energies of sextet, quartet and doublet states were computed; and for the Fe(IV) complexes, the energies of quintet and triplet states were calculated. For the two Fe(IV) complexes studied here we considered two conformations of the macrocyclic ring with the two N–CH_2–CH_2–N groups in a parallel or crossed orientation. These conformations are based on available crystallographic data for the $[Fe(O)(TMC)(MeCN)]^{2+}$ complex[85] and two related oxoiron(IV) complexes with TMC-based ligands.[86,87] In the manuscript we report spin state splitting energies for the lowest-energy conformers. Relative energies of the high-energy conformers and representative depictions of the conformations are given in Section 2 of the ESI.†

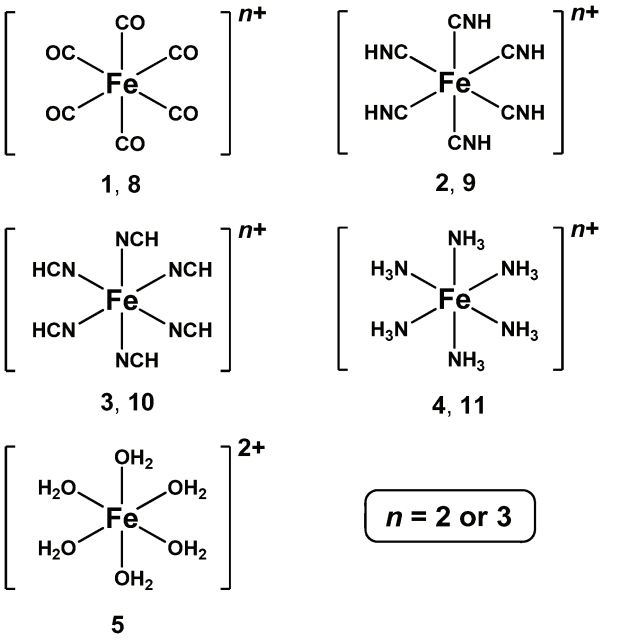

Fig. 1 The structures of iron complexes **1–5** and **8–11**.

Complexes **6**, **7** and **12** have served as challenging examples of large molecular complexes for accurate predictions of spin state splitting energies by KS-DFT in previous studies such as ref. 45.

3 Computational methods

KS-DFT was employed to calculate the electronic structure of Fe^{2+} ion, gaseous FeO and 14 iron complexes, and WFT was employed to treat nine of the 14 complexes. All calculations were carried out for the gas-phase isolated molecules or ions. The symmetry used in our calculations is $C_{\infty v}$ or C_{2v} for FeO (based on the maximum available symmetry operation in the program used) and C_1 for the 14 iron complexes.

KS-DFT

The density functional calculations on all the compounds were performed with the *Gaussian 09*[88,89] program and a locally modified version[90] of it. We used 20 exchange–correlation functionals, as listed in Table 1. Table 1 also gives the types of the functionals, the percentages X of HF exchange and the ref. 58, 66, 68, 81, 83 and 91–108. These functionals were selected for study for various

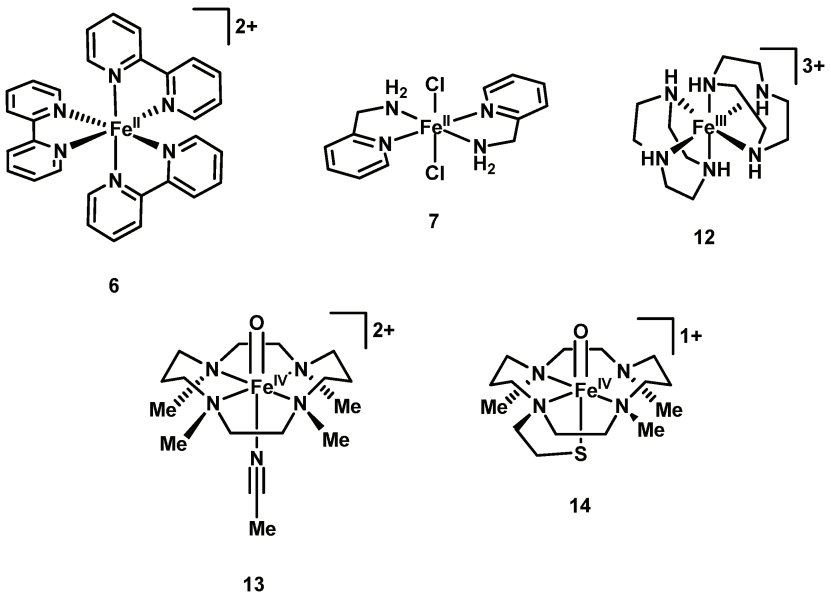

Fig. 2 The structures of iron complexes **6**, **7** and **12–14**.

reasons, including popularity and success in our previous[56,104] tests, or those of others, as noted in the introduction.

The geometries were optimized for all the spin states using an ultrafine grid (that has 99 radial shells around each atom, each shell having 590 angular points) or a larger grid that has 96 radial shells around each atom, each shell having 32 points in θ and 64 points in ϕ.

A triple-zeta basis set, def2-TZVP (valence-triple-zeta basis set with polarization)[109] was used in all cases except where stated otherwise. For a few cases, ma-TZVP (where ma- denotes a minimally augmented[110] def2 basis set), ma-TZVPP,[110] def2-QZVP,[109] ma-QZVP,[110] def2-QZVPP,[109] ma-QZVPP,[110] cc-pVTZ,[111] cc-pVTZ-DK,[112] cc-pVQZ-DK,[112] cc-pwCVTZ-DK[112] and cc-pwCVQZ-DK[112] basis sets were also used, as noted in those cases. After geometry optimizations, the stability of the single Slater determinant wave functions were tested, and if found unstable, allowed to converge to the most stable, possibly broken-symmetry,[51,113,114] solutions.[88–90] Hessian analyses were performed in order to confirm that all structures are minima on the potential energy surfaces. A few cases had small imaginary frequencies ($<$20i cm^{-1}) corresponding to the methyl rotation of MeCN in complex **13**, and these low imaginary frequencies were ignored.

Table 1 Density functionals tested

Functional	Type[a]	X[b]	Ref.
GVWN5[c]	LSDA	0	91–94
BLYP	GGA	0	68 and 81
PBE	GGA	0	67
OPBE	GGA	0	66 and 67
OLYP	GGA	0	66 and 68
N12	NGA	0	95
GAM	NGA	0	96
M06-L	MGGA	0	97
M11-L	Range-separated MGGA	0	98
MN15-L	MNGA	0	99
B3LYP*	Hybrid GGA	15	58
B3LYP[d]	Hybrid GGA	20	68, 81, 83 and 100
PBE0[e]	Hybrid GGA	25	101
B97-3	Hybrid GGA	26.93	106
M06	Hybrid MGGA	27	103
PW6B95	Hybrid MGGA	28	107
SOGGA11-X	Hybrid GGA	35.42	102
MPW1B95	Hybrid MGGA	31	105
MN15	Hybrid MNGA	44	104
M08-SO	Hybrid MGGA	56.79	108

[a] Abbreviations: local spin-density approximation (LSDA), generalized gradient approximation (GGA), nonseparable gradient approximation (NGA), meta-GGA (MGGA), meta-NGA (MNGA). [b] X denotes the percentage of HF exchange. [c] The keyword for this method is SVWN5 in *Gaussian 09* and LDA in *Molpro*. [d] The keyword for this method is B3LYP in *Gaussian 09* and B3LYP3 in *Molpro*. [e] The keyword for this method is PBE1PBE in *Gaussian 09* and PBE0 in *Molpro*.

Only for FeO, spin-unrestricted DFT calculations were also done using *Molpro* version 2015.1.10[115] in C_{2v} symmetry with 10 of the 20 functionals tested in this work. In the radial part of the integration grid the degrees of quadrature was set to 99 for each atom and the convergence criterion for optimization was set equivalent to that of *Gaussian*.

WFT

We computed the spin–orbit coupling[116] terms for the nine smallest Fe(II) and Fe(III) complexes. These calculations were performed using *Molpro* version 2010.1.24[115] and were single-point calculations on the GAM/def2-TZVP optimized geometries. State-averaged complete active space self-consistent field (SA-CASSCF)[117–123] calculations without spin–orbit coupling were followed by state-interaction calculations,[124–126] where the spin–orbit eigenstates are obtained by diagonalizing $\hat{H}_{el} + \hat{H}_{SO}$ (the subscript "el" labels the spin-free electronic Hamiltonian, and the subscript "SO" indicates the spin–orbit interaction Hamiltonian) in a basis of eigenfunctions of $\hat{H}_{el}$ for internal configurations of the active space, and the contributions of external configurations were approximated by mean-field

one-electron Fock operator. The correlation-consistent polarized double-zeta basis set, cc-pVDZ[111,127] was used in these spin–orbit calculations. Two cases, quintet $[Fe(CNH)_6]^{2+}$ and doublet $[Fe(CNH)_6]^{3+}$, were tested using a larger basis set, cc-pVTZ. The spin–orbit couplings changed by no more than a few wavenumbers as compared to the cc-pVDZ basis set results. Hence all spin–orbit coupling values reported in this work are with the cc-pVDZ basis set. The active space used for the Fe(II) complexes includes six electrons in five 3d orbitals (6/5), and the active space used for the Fe(III) complexes includes five electrons in five 3d orbitals (5/5). Thus, we placed six electrons in the five d orbitals of Fe(II) and five electrons in the five 3d orbitals of Fe(III), respectively. The symmetry was turned off during the SA-CASSCF calculations, wherein initially five equally weighted states were investigated. This was followed by increasing the number of states to 10 and 20 equally weighted states for doublet Fe(III) complexes as described in Section 4.2. For the nine complexes, the energy splitting between two spin states is also calculated by adding the spin–orbit coupling energy for each complex to its total electronic energy.

4 Results and discussion

Although solvation and other environmental effects can be important in condensed-phase studies, the present study is based entirely on gas-phase calculations. Although solvation would change the quantitative values of spin splittings, it is not expected to change our major conclusions.

4.1 Performance of exchange–correlation functionals without including spin–orbit coupling

In Table 2, the spin-state splitting energies for the Fe^{2+} ion are presented and compared to the experimental[128] values.

In Table 3, spin-state splitting energies, harmonic frequencies, bond lengths and dipole moments of gaseous FeO are presented and compared to experimental data where available. Table 4 presents splitting energies and bond lengths for 10 functionals calculated in *Molpro*. In some cases these results differ slightly from those in Table 3; this is because *Gaussian 09* allows spatial symmetry breaking to achieve a stable solution, while in *Molpro* the spatial symmetry is maintained during the calculation.

In Tables 5–7, we show the calculated spin-state splitting energies of Fe(II), Fe(III) and Fe(IV) complexes, respectively. Note that for each structure, the geometries of the different spin states are separately optimized for every spin state, and hence the reported values are the adiabatic (not the vertical) electronic energy splittings. In the absence of experimental values of spin-state splitting energies, Tables 5–7 contain the reference ground spin states,[39,43,129–132] and their last columns give the number of correct predictions of the ground state for each density functional.

This section considers only calculations without spin–orbit coupling.

4.1.1 Fe^{2+} ion. Monatomic ions present unique issues that molecules without degeneracies do not have, but they also provide challenges that should not be ignored.

Table 2 Calculated and experimental spin-state splitting energies[a] (kcal mol^{-1}) of the Fe^{2+} ion

Functional	$E_{singlet} - E_{quintet}$	$E_{triplet} - E_{quintet}$	$E_{singlet} - E_{triplet}$
GVWN5	59.9	44.2	15.7
BLYP	42.1	34.6	7.5
PBE	46.7	38.0	8.7
OPBE	62.8	48.9	13.9
OLYP	59.1	45.7	13.4
N12	42.0	34.6	7.4
GAM	80.7	58.6	22.1
M06-L	48.0	44.8	3.2
M11-L	−19.5	7.9	−27.4
MN15-L	94.5	72.2	22.3
B3LYP*	46.6	37.7	8.9
B3LYP	46.4	37.8	8.6
PBE0	50.6	41.3	9.3
B97-3	49.1	39.3	9.8
M06	73.1	47.5	25.6
PW6B95	50.6	39.7	10.9
SOGGA11-X	56.7	44.2	12.5
MPW1B95	54.1	42.1	12.0
MN15	28.9	28.7	0.2
M08-SO	51.0	42.6	8.4
Expt.[b]	85.6	56.1	29.5

[a] Spin–orbit coupling was not included in calculating spin-state splitting energies. [b] Experimental values are taken from ref. 128, where the spin-split energies were converted back to spin-free representation.

The calculated quintet states are pure spin states as indicated by $\langle S^2 \rangle$ value of 6.0 with all 20 functionals. With a few functionals, we switched orbitals and found that the total electronic energy is unaffected by how the only beta electron is paired with any of the five alpha electrons.

The calculated triplet states are not pure spin states as indicated by $\langle S^2 \rangle$ values lying in the range 2.73–3.00 for all 20 functionals. The Slater determinants of SVWN5 (intermediate $\langle S^2 \rangle$ value) and MN15 (highest $\langle S^2 \rangle$ value) were used as initial guesses for the MN15-L (lowest $\langle S^2 \rangle$ value) calculation. We found that the Slater determinants of SVWN5 and MN15 are similar to each other, and that of MN15-L is different from them, but the final energies of the MN15-L calculations obtained with and without SVWN5 and MN15 Slater determinants as initial guesses are the same due to the use of "stable = opt" option in *Gaussian 09*. As discussed above, in all cases we used the "stable = opt" option in *Gaussian 09*. In addition, we often try more than one initial guess. The energy we quote is always the variationally lowest energy for that spin state and that functional, and this provides a consistent way to do the comparisons, as discussed in a previous paper.[56]

The calculated singlet states also are not pure spin states as indicated by $\langle S^2 \rangle$ values lying in the range 1.83–1.98 for all 20 functionals. But again the energy we quote is always the variationally lowest energy for that spin state and that functional, and this again provides a consistent way to do the comparisons.

Table 2 shows that all functionals except M11-L correctly predict the ground spin state of the Fe^{2+} ion to be quintet. However, if we compare the magnitude of $E_{singlet} - E_{quintet}$ splittings to experiments, most of the functionals significantly deviate from the experimental values, significantly underestimating the spin-state splitting energies. Of the functionals tested, the GAM

Table 3 Calculated and experimental equilibrium bond lengths (r_e in Å), dipole moments (μ in D), harmonic frequencies (ω in cm^{-1}), and spin splittings (ΔE in kcal mol^{-1}) of FeO. These calculations are carried out with *Gaussian 09*, and the spin-state splitting energies[a] of the quintet ($^5\Sigma$) and the septet ($^7\Sigma$) states are computed with respect to the $^5\Delta$ state

	$^5\Delta$ ($3d\sigma 3d\pi^2 3d\delta^3$)			$^5\Sigma$[b] ($3d\sigma^2 3d\pi^2 3d\delta^2$)				$^7\Sigma$ ($3d\sigma 3d\pi^2 3d\delta^2 4s\sigma$)			
Functional	r_e	μ	ω	r_e	μ	ω	ΔE	r_e	μ	ω	ΔE
GVWN5	1.580	4.19	971	—	—	—	—	1.657	2.05	867	27.0
BLYP	1.618	4.35	895	—	—	—	—	1.705	2.23	775	28.3
PBE	1.604	4.29	920	—	—	—	—	1.685	2.12	812	25.1
OPBE	1.591	4.48	931	—	—	—	—	1.667	1.96	836	19.2
OLYP	1.607	4.52	902	1.637	3.85	875	11.4	1.686	2.09	798	22.9
N12	1.593	4.53	930	—	—	—	—	1.680	1.95	782	33.1
GAM	1.618	4.11	873	1.638	3.77	869	6.9	1.687	2.32	784	18.0
M06-L	1.614	4.39	918	1.627	3.94	925	6.8	1.681	2.55	828	20.2
M11-L	1.570	4.89	981	—	—	—	—	1.659	2.23	810	40.4
MN15-L	1.612	4.57	937	1.622	3.93	950	4.5	1.670	2.86	873	8.0
B3LYP*	1.606	4.92	915	1.628	4.22	916	10.3	1.681	2.50	820	23.4
B3LYP	1.608	5.13	910	1.627	4.38	922	10.2	1.679	2.60	821	22.0
PBE0	1.598	5.27	922	1.615	4.54	949	12.3	1.660	2.63	864	17.2
B97-3	1.611	5.53	899	1.623	4.64	930	8.5	1.668	2.71	843	21.9
M06	1.610	5.59	925	1.616	4.17	950	−5.5	1.666	2.71	867	17.6
PW6B95	1.603	5.39	912	1.618	4.56	941	10.1	1.665	2.67	845	20.0
SOGGA11-X	1.611	5.87	899	1.611	4.82	970	4.2	1.660	2.91	869	17.2
MPW1B95	1.600	5.49	916	1.614	4.60	954	9.7	1.658	2.71	864	18.0
MN15	1.597	5.61	942	1.614	4.62	949	6.6	1.656	2.41	878	19.2
M08-SO	1.638	6.51	861	1.622	5.39	954	1.7	1.668	3.26	870	11.2
Expt.	1.618[c]	4.50[d]	882[e]	1.625[f]	—	800[e] (881)[f]	11.6[e] (5.9)[g]	—	—	877[e]	3.3[e] (14.2)[g]

[a] Spin–orbit coupling was not included in calculating spin-state splitting energies. [b] The $^5\Sigma$ state was not determined for some of the functionals. [c] r_0 value is using rotational spectroscopy (ref. 156), and converted to r_e as described in the ESI. [d] Ref. 157. [e] Ref. 158. [f] r_0 value is using rotational spectroscopy (ref. 159), and converted to r_e as described in the ESI. [g] Ref. 160.

Table 4 Calculated bond lengths (r_e in Å) and spin splittings (ΔE in kcal mol^{-1}) of FeO using 10 density functionals in *Molpro*. The spin-state splitting energies[a] of the quintet ($^5\Sigma$) and the septet ($^7\Sigma$) states are computed with respect to the $^5\Delta$ state

	$^5\Delta$	$^5\Sigma$		$^7\Sigma$	
Functional	r_e	r_e	ΔE	r_e	ΔE
GVWN5[b]	1.580	1.607	10.8	1.657	27.0
BLYP	1.618	1.645	11.1	1.705	28.3
PBE	1.604	1.632	13.4	1.685	25.1
M06-L	1.606	1.626	7.3	1.673	20.7
M11-L	1.591	1.611	30.9	1.685	41.2
B3LYP[c]	1.608	1.627	10.2	1.679	22.0
PBE0	1.598	1.615	12.2	1.660	17.1
M06	1.601	1.610	−4.8	1.654	18.3
SOGGA11-X	1.611	1.611	4.2	1.660	17.2
M08-SO	1.620	1.621	2.1	1.666	11.6

[a] Spin–orbit coupling was not included in calculating spin-state splitting energies. [b] The keyword for this method is SVWN5 in *Gaussian 09* and LDA in *Molpro*. [c] The keyword for this method is B3LYP in *Gaussian 09* and B3LYP3 in *Molpro*.

value of 80.7 kcal mol^{-1} is closest to experiments, and is off from experiment by 4.9 kcal mol^{-1}. We note, however, that the primary source of error in most of the functionals appears to be associated with the highest-energy spin state, the singlet, as the triplet–quintet splitting is predicted by most functionals to be in the 40–50 kcal mol^{-1} range, which is in considerably better agreement with the experimental value of 56.1 kcal mol^{-1}. Again, here, GAM gives the best agreement with experiments differing by only 2.5 kcal mol^{-1} from it. Evidently, all functionals overstabilize lower spin states compared to higher spin states for this atomic ion, with the effect being most profound for the singlet.

Monatomic ions with a given oxidation state, in this case oxidation state 2, are not necessarily representative of that oxidation state in polyatomic molecules or ions, and we next turn to polyatomic molecules and ions for cases more relevant to practical applications.

4.1.2 Gaseous FeO. FeO is the simplest molecule in which Fe is in oxidation state 2. In Table 3, spin splittings (in kcal mol^{-1}), bond lengths (in Å), harmonic frequencies (in cm^{-1}) and dipole moments (in D) of FeO are presented. Since there is more than one quintet state of FeO, we present the two lowest energy quintets as shown by experiments, in particular, the $^5\Delta$ and $^5\Sigma$ states. For some of the functionals (especially the local functionals), the $^5\Sigma$ state could not be determined, and for those functionals only the $^5\Delta$ state is presented. The experimental bond lengths for these two states in the table are r_e values obtained from the corresponding r_0 values, and the procedure to extract r_e from r_0 is described in detail in the ESI.†

For the functionals for which the $^5\Sigma$ state could be determined, the calculated bond lengths increase (r_e) as one goes from $^5\Delta$ to $^5\Sigma$ to $^7\Sigma$ state (with the exception of M08-SO), and the calculated dipole moments decrease in the same order. The functionals that predict the best r_e values for the $^5\Delta$ state of FeO are BLYP, GAM, M06-L, MN15-L, SOGGA11-X, B97-3 and M06, where the difference from experiments is within 0.010 Å. The geometry of the $^7\Sigma$ state is not available from experiments, but multireference WFT calculations by Sakellaris *et al.*[133] predict that the Fe–O bond for the septet state is longer than that of both the quintet states,

Table 5 Calculated spin-state splitting energies[a] (kcal mol^{-1}) of seven Fe(II) complexes

Functional	State[b]	**1** $[Fe(CO)_6]^{2+}$	**2** $[Fe(CNH)_6]^{2+}$	**3** $[Fe(NCH)_6]^{2+}$	**4** $[Fe(NH_3)_6]^{2+}$	**5** $[Fe(H_2O)_6]^{2+}$	**6** $[Fe(bipy)_3]^{2+}$	**7** $Fe(amp)_2Cl_2$	Number of correct predictions
GVWN5	Triplet	76.8	80.5	42.5	23.6	5.9	40.6	21.1	4/7
	Quintet	119.2	129.9	56.8	25.2	−7.9	60.0	31.8	
BLYP	Triplet	47.6	53.0	21.5	9.4	−0.1	22.9	9.5	4/7
	Quintet	64.4	76.1	18.6	1.1	−20.3	25.8	5.6	
PBE	Triplet	57.4	62.3	25.4	10.6	−0.5	26.2	10.9	4/7
	Quintet	80.3	91.4	23.8	1.2	−23.0	30.9	8.5	
OPBE	Triplet	59.9	64.7	20.0	−4.9	−8.6	19.8	5.6	6/7
	Quintet	75.3	87.1	6.3	−18.7	−44.2	13.5	−7.6	
OLYP	Triplet	48.9	54.5	15.6	−4.5	−7.8	16.8	3.7	6/7
	Quintet	57.6	70.4	0.8	−18.0	−41.1	8.9	−10.7	
N12	Triplet	61.8	67.5	30.9	17.2	4.4	31.3	16.7	4/7
	Quintet	91.8	104.3	37.8	17.3	−9.0	43.1	21.0	
GAM	Triplet	38.5	44.5	7.1	−4.1	−14.1	10.0	−4.6	6/7
	Quintet	35.4	48.3	−19.9	−35.0	−58.7	−8.6	−28.7	
M06-L	Triplet	41.4	46.4	17.9	8.7	−0.1	21.1	7.0	6/7
	Quintet	43.3	53.5	2.8	−10.6	−30.5	11.3	−8.9	
	Septet[c]	136.1	137.8	86.1	95.2	82.4			
M11-L	Triplet	60.8	65.0	46.3	37.0	31.8	47.4	34.4	3/7
	Quintet	88.0	97.5	63.6	50.7	39.5	69.2	49.0	
MN15-L	Triplet	34.9	40.8	8.0	0.1	−10.9	14.3	−1.6	6/7
	Quintet	20.3	32.0	−24.4[f]	−34.2	−57.6	−9.1	−30.8	
B3LYP*	Triplet	38.7	45.0	15.5	6.8	−1.3	17.0	5.3	6/7
	Quintet	42.9	56.1	4.2	−8.0	−26.2	10.2	−8.1	
B3LYP	Triplet	32.6	39.2	12.1	4.9	−1.8	13.6	11.5	7/7
	Quintet	30.8	44.2	−3.1	−12.6	−28.2	2.6	−14.1	
PBE0	Triplet	35.9	42.4	10.9	3.1	−3.0	12.6	1.7	6/7
	Quintet	31.9	45.7	−8.6	−19.2	−33.2	−2.1	−19.6	
B97-3	Triplet	27.4	34.4	7.3	1.8	−3.8	9.6	0.6	6/7
	Quintet	17.8	31.9	−13.9	−20.6	−34.1	−7.3	−22.4	
M06	Triplet	29.2	35.9	7.4	0.1	−10.5	10.5	−1.7	6/7
	Quintet	22.9	36.1	−13.2	−22.8	−45.1	−5.3	−24.2	
PW6B95	Triplet	32.1	39.0	12.0	5.9	−2.2	14.5	3.7	7/7
	Quintet	27.7	41.5	−4.6	−12.4	−29.7	2.9	−14.3	
SOGGA11-X	Triplet	22.1	28.6	6.1	2.1	−3.6	8.4	−0.1	6/7
	Quintet	7.7	20.3	−17.9	−22.7	−36.2	−12.1	−26.6	
MPW1B95	Triplet	32.7	39.5	11.7	5.5	−2.9	14.4	3.3	7/7
	Quintet	26.9	40.9	−6.3	−14.6	−32.3	1.2	−16.3	
MN15	Triplet	28.5	35.9	4.6	−2.9	−2.4	9.1	−4.0	7/7
	Quintet	33.1	47.7	−4.3	−14.2	−23.0	5.9	−13.5	
M08-SO	Triplet	3.5	10.0	−8.2	−10.6	−9.9	−4.2	−10.8	4/7
	Quintet	−19.3	−6.8	−38.9[f]	−41.3	−46.7	−29.4	−42.9	
Reference ground spin state		Singlet[d]	Singlet[e]	Quintet[d]	Quintet[d]	Quintet[d]	Singlet[g]	Quintet[h]	

[a] Spin–orbit coupling was not included in calculating spin-state splitting energies for this table. [b] If this column says triplet, the row shown is $E_{triplet} - E_{singlet}$, if this column says quintet, the row shown is $E_{quintet} - E_{singlet}$, and if this column says septet, the row shown is $E_{septet} - E_{singlet}$. [c] The septet state was calculated only for complexes **1–5** with the M06-L exchange–correlation functional. [d] The reference ground spin state is based on diffusion Monte Carlo (DMC) calculations reported in ref. 39. [e] The reference ground spin state is based on approximations from ligand-field theory. [f] The most stable wave function could not be obtained. [g] The reference ground spin state is based on best experimental estimate reported in ref. 43. [h] The reference ground spin state is based on experimental investigations in ref. 129.

which is in agreement with all the KS-DFT calculations in this work. The difference in experimental bond lengths of the $^5\Delta$ and $^5\Sigma$ states is 0.006 Å, indicating that there is a negligible difference in their bond lengths, which is similar to what is predicted by all the functionals here, where we find that the maximum difference in bond lengths for the two states is no more than 0.030 Å (obtained with OLYP). The experimental dipole moment is available only for the $^5\Delta$ state of FeO and the top five functionals that agree with the experimental value of 4.50 D are OPBE, OLYP, N12, M06-L and MN15-L.

If we compare spin-state splitting energies we find that all functionals predict the ground spin state to be a quintet, which agrees with experiments.[134] The calculated values show that $^5\Delta$ is the ground state for all the functionals except M06, which predicts $^5\Sigma$ as the ground state. According to the experimental values reported by Drechsler *et al.*,[158] the $^7\Sigma$ state is next higher in energy after the $^5\Delta$ state, and the excitation energy is 3.3 kcal mol^{-1}. In comparison to their experiment, we find that all functionals overestimate the energy of the $^7\Sigma$ state with respect to the $^5\Delta$ state and predict the $^7\Sigma$ state to be at least 8.0 kcal mol^{-1} (obtained with MN15-L) higher in energy than the $^5\Delta$ state. Moreover, from these experiments, the $^5\Sigma$ state is higher in energy than the $^7\Sigma$ state, but the functionals that predicted the existence of the $^5\Sigma$ state all show an opposite trend. However, a more recent experiment by Kim *et al.*[160] reassigned the states and found that the $^5\Sigma$ state is lower in

Table 6 Calculated spin-state splitting energies[a] (kcal mol^{-1}) of five Fe(III) complexes

Functional	State[b]	**8** $[Fe(CO)_6]^{3+}$	**9** $[Fe(CNH)_6]^{3+}$	**10** $[Fe(NCH)_6]^{3+}$	**11** $[Fe(NH_3)_6]^{3+}$	**12** $[Fe([9]aneN_3)_2]^{3+}$	Number of correct predictions
GVWN5	Quartet	50.7	60.1	27.9	−39.8	28.6	3/5
	Sextet	78.2	96.7	34.6	−30.0	41.8	
BLYP	Quartet	27.4	36.7	13.6	11.0	17.9	3/5
	Sextet	38.0	55.3	9.0	13.9	24.1	
PBE	Quartet	33.8	43.2	15.6	11.5	19.0	3/5
	Sextet	47.1	65.0	11.2	13.6	25.1	
OPBE	Quartet	29.4	40.2	7.5	1.6	10.3	5/5
	Sextet	32.5	52.8	−8.7	−7.1	7.1	
OLYP	Quartet	21.9	32.6	5.1	1.3	9.2	5/5
	Sextet	22.3	42.0	−11.4	−6.4	6.4	
N12	Quartet	39.9	50.1	22.6	19.2	25.9	3/5
	Sextet	61.3	80.5	27.1	30.4	38.5	
GAM	Quartet	11.2	21.6	−5.3	−8.1	−1.0	4/5
	Sextet	2.2	20.6	−33.9	−25.5	−11.6	
M06-L	Quartet	17.5	25.9	5.4	5.4	11.5	5/5
	Sextet	8.7	24.2	−19.5	−11.1	3.9	
M11-L	Quartet	49.7	57.5	43.5	40.7	45.6	3/5
	Sextet	68.6	84.0	52.3	53.4	65.6	
MN15-L	Quartet	3.8	14.1	−10.1	−10.2	−0.5	2/5
	Sextet	−20.5	−3.0	−53.4	−41.1	−18.7	
B3LYP*	Quartet	20.5	29.7	9.3	7.4	13.9	4/5
	Sextet	22.5	39.8	−2.2	3.4	16.7	
B3LYP	Quartet	16.5	25.4	6.9	7.5	11.7	5/5
	Sextet	14.3	31.3	−7.9	−1.5	11.7	
PBE0	Quartet	16.6	26.0	4.8	2.9	9.5	5/5
	Sextet	11.1	28.8	−14.5	−8.7	5.5	
B97-3	Quartet	11.5	20.6	2.7	1.6	8.0	5/5
	Sextet	2.9	19.8	−18.1	−10.9	2.9	
M06	Quartet	8.4	17.5	−2.8	−2.8	3.3	3/5
	Sextet	−2.7	14.3	−30.0	−21.2	−6.6	
PW6B95	Quartet	15.9	24.9	6.4	5.3	12.5	5/5
	Sextet	11.8	28.9	−10.1	−3.4	11.7	
SOGGA11-X	Quartet	8.4	16.6	0.5	0.1	6.2	3/5
	Sextet	−4.7	11.0	−25.0	−17.0	−3.2	
MPW1B95	Quartet	15.3	24.4	5.3	4.0	11.5	5/5
	Sextet	9.2	26.7	−13.3	−6.9	8.7	
MN15	Quartet	16.5	25.5	5.1	4.8	12.1	4/5
	Sextet	24.6	42.6	−0.6	6.2	21.6	
M08-SO	Quartet	−5.0	2.6	−10.6	−10.6	−5.1	2/5
	Sextet	−24.8	−9.0	−43.5	−34.6	−20.5	
Reference ground spin state		Doublet[c]	Doublet[c]	Sextet[c]	Sextet[c]	Doublet[d]	

[a] Spin–orbit coupling was not included in calculating spin-state splitting energies for this table. [b] If this column says quartet, the row shows $E_{quartet} - E_{doublet}$, and if this column says sextet, the row shows $E_{sextet} - E_{doublet}$. [c] The reference ground spin state is based on approximations from ligand-field theory. [d] The reference ground spin state is based on experiments in ref. 130.

energy than the $^7\Sigma$ state, which is in agreement with the prediction of all the functionals. Furthermore the theoretical excitation energies agree better with the newer experiment than with the older one.

As mentioned above, there are some local functionals for which the $^5\Sigma$ state was not calculated with *Gaussian 09*. To calculate these states we used *Molpro*, which allows specification of irreducible representations of C_{2v} symmetry for FeO. The results for ten of the functionals are given in Table 4. The conclusions from Table 4 are similar to what has been already discussed.

4.1.3 Hexacoordinate Fe complexes. In Table 5, the energy splittings of seven hexacoordinate Fe(II) complexes are presented. We see that for complexes $[Fe(CO)_6]^{2+}$ and $[Fe(CNH)_6]^{2+}$, all density functionals correctly predict the ground spin state to be a singlet, except for M08-SO, which predicts quintet to be ground spin state. It appears that the overstabilization of the quintet spin state by the M08-SO functional may be attributed to its high percentage of HF exchange (56.79%), and in fact functionals with this high amount of HF exchange were not originally intended for use on transition metals (although this functional is included here to illustrate the kind of performance one can obtain with high HF exchange because it turns out[56,104] that sometimes functionals with high HF exchange can give useful results for transition metals). For $[Fe(NCH)_6]^{2+}$, the ground spin state is a quintet, which is correctly predicted by two of the local functionals, GAM and MN15-L, and by all hybrid functionals except B3LYP*. For $[Fe(NH_3)_6]^{2+}$ and $Fe(amp)_2Cl_2$, the ground spin state is again a quintet, which is correctly predicted by three local functionals, namely GAM, M06-L and MN15-L, and by all hybrid functionals. For $[Fe(H_2O)_6]^{2+}$, all functionals except for M11-L correctly predict the quintet to be the ground spin state. For the $[Fe(bipy)_3]^{2+}$ complex, all the local functionals except GAM and MN15-L correctly predict it to possess a singlet ground state. This means

Table 7 Calculated spin-state splitting energies[a] $E_{quintet} - E_{triplet}$ (kcal mol^{-1}) of two Fe(IV) complexes

Functional	**13** $[Fe(O)(TMC)(MeCN)]^{2+}$	**14** $[Fe(O)(TMCS)]^{+}$	Number of correct predictions
GVWN5	23.1	18.3	2/2
BLYP	12.0	7.2	2/2
PBE	12.9	8.3	2/2
OPBE	2.9	−1.8	1/2
OLYP	2.3	−3.1	1/2
N12	19.9	15.5	2/2
GAM	−4.8	−11.8	0/2
M06-L	3.4	−2.1	1/2
M11-L	35.9	32.7	2/2
MN15-L	−9.5	−16.2	0/2
B3LYP*	7.0	1.8	2/2
B3LYP	4.3	−1.0	1/2
PBE0	1.6	−3.6	1/2
B97-3	−0.3	−5.8	0/2
M06	−5.6	−12.5	0/2
PW6B95	5.5	0.4	2/2
SOGGA11-X	−4.2	−9.5	0/2
MPW1B95	4.2	−0.9	1/2
MN15	6.1	0.3	2/2
M08-SO	−16.1	−20.6	0/2
Reference ground spin state	Triplet[b]	Triplet[c]	

[a] Spin–orbit coupling was not included in calculating spin-state splitting energies. A positive value of $E_{quintet} - E_{triplet}$ indicates that the triplet state is the ground spin state. [b] The reference ground spin state is based on experiments in ref. 85. [c] The reference ground spin state is based on experiments in ref. 131.

that even though GAM and MN15-L are local functionals, they have a tendency to stabilize the quintet state. Overall we find that the hybrid functionals, B3LYP, PW6B95, MPW1B95 and MN15 correctly predict the ground spin state of all seven Fe(II) complexes, and five local functionals, OPBE, OLYP, GAM, M06-L and MN15-L and five hybrid functionals, B3LYP*, PBE0, B97-3, M06 and SOGGA11-X, predict the correct spin state for six out of seven complexes.

In Table 6, the energy splittings of five hexacoordinate Fe(III) complexes are shown. Table 6 shows that $[Fe(CO)_6]^{3+}$ and $[Fe(CNH)_6]^{3+}$ are doublets, and all local functionals except MN15-L predict their correct spin state. All hybrid functionals except SOGGA11-X, M06 and M08-SO correctly predict it to be doublet for $[Fe(CO)_6]^{3+}$ and all hybrid functionals except M08-SO correctly predict $[Fe(CNH)_6]^{3+}$ to be doublet. The complex $[Fe(NCH)_6]^{3+}$ has a sextet ground state, and this is correctly predicted by the OPBE, OLYP, GAM, M06-L and MN15-L local functionals, and by all the hybrid functionals. The complex $[Fe(NH_3)_6]^{3+}$ is also a sextet, and again the OPBE, OLYP, GAM, M06-L and MN15-L local functionals correctly predict that, while the only hybrid functionals that do not predict it correctly are B3LYP* and MN15. The $[Fe([9]aneN_3)_2]^{3+}$ complex is a doublet, and only the GAM and MN15-L local functionals and the M06, SOGGA11-X and M08-SO hybrid functionals are not able to predict the correct ground spin state. For the five Fe(III) complexes overall, the OPBE, OLYP and M06-L local functionals and the B3LYP, PBE0, B97-3, PW6B95 and MPW1B95 hybrid functionals predict the correct ground spin state for all complexes.

Iron(IV)–oxo complexes have been demonstrated to show both hydrogen atom transfer (HAT) and oxygen atom transfer (OAT) reactivity, as for example demonstrated by Sastri *et al.* for a series of synthetic nonheme TMC-based Iron(IV)–oxo complexes.[135] This type of reactivity has been rationalized with the two-state reactivity principle[34,35] for non-heme Fe(IV)–O complexes bearing ligands of the TMC family,[135–137] leading to a situation where the accurate prediction of spin-state splitting energies is crucial to the computational analysis of reactivity. The two-state reactivity model has been associated with non-heme Fe(IV)–O complexes which possess a triplet ground spin state, which is the most commonly encountered spin state for synthetic model complexes of this type,[138,139] as reactions proceeding on the high-spin surface benefit from exchange enhanced reactivity.[140,141] For our study here, we selected the structurally related complexes $[Fe^{IV}(O)(TMC)(MeCN)]^{2+}$ and $[Fe^{IV}(O)(TMCS)]^{+}$, which differ in having the ligand trans to the oxo atom being a solvent molecule (MeCN) or a thiolate that is tethered to the TMC backbone, because their spin ground states have been unequivocally determined to be triplets by Mössbauer spectroscopy.[85,131] Previous computational studies have shown that the correct prediction of the spin ground state has proven challenging for the $[Fe^{IV}(O)(TMCS)]^{+}$ complex.[135–137,142,143] Table 7 shows that all the local functionals except OPBE, OLYP, GAM, M06-L and MN15-L correctly predict $[Fe(O)(TMCS)]^{+}$ to possess a triplet ground spin state, but we note that (of course) getting the state-energy splitting right does not guarantee a functional can model the reactivity, ionization potential, dipole moment, or any other property of iron(IV)–oxo complexes.[141,144] B3LYP*, PW6B95 and MN15 are the only hybrid functionals that correctly predict the triplet to be lower in energy than the quintet, but only by a small amount (<2 kcal mol^{-1}). We find that more functionals predict the $[Fe(O)(TMC)(MeCN)]^{2+}$ complex to be a triplet than is the case for $[Fe(O)(TMCS)]^{+}$, as might be expected given the stronger ligand field associated with the former complex compared to the latter.

One of the NGA functionals used in this work, N12, predicts the ground spin state of four of the seven Fe(II) complexes, three of the five Fe(III) complexes and both the Fe(IV) complexes correctly. In contrast, the other NGA, which is the more recent GAM functional, which has the same functional form as N12, but which has been optimized with smoothness constraints with a larger set of transition metal data, gives correct predictions for all of the Fe(II) and Fe(III) complexes except two, but not for the two Fe(IV) complexes.

The use of hybrid GGAs (B3LYP, B3LYP*, PBE0 and SOGGA11-X) does improve the predictions in Tables 5 and 6. This supports some previous findings,[58–62,145] which found that introduction of small amounts of HF exchange (10–27%) can significantly improve the prediction of the ground states of spin crossover complexes. The spin-state splitting energies obtained by B3LYP and PBE0 are quite similar to each other.

The introduction of kinetic energy density terms in meta GGAs or meta NGAs allows one to reduce self-interaction energy and self-correlation energy in regions dominated by a single spatial orbital.[107,146] The M06-L meta-GGA functional correctly predicts the ground spin state of 12 of the 14 complexes, consistent with its good performance in a previous[145] study. Two of the complexes, $[Fe(NCH)_6]^{2+}$ and $[Fe(O)(TMCS)]^{+}$, for which the prediction of M06-L is not correct are discussed in greater detail in Section 4.4. For these complexes, the spin splitting energies from M06-L are small values (2.8 kcal mol^{-1} and –2.1 kcal mol^{-1}, respectively), and they are tested to understand the effect of the basis set. In addition to the quintet, triplet and singlet states, we calculated the septet state for complexes **1–5** in Table 5 with the M06-L functional. This is because in Table 3, the experimental data shows that the energy of the septet state of FeO is only 3.3 kcal mol^{-1} higher than the lowest quintet state ($^5\Delta$ state). Hence this motivated us to compute the septet state of complexes **1–5**, and unlike FeO, all the five complexes give the energy of the septet state to be much higher than the quintet state.

In contrast to the good results obtained with M06-L, Tables 5–7 show that the M11-L meta-GGA functional gives a positive splitting for every complex. With our sign convention, this indicates that M11-L predicts the low-spin state (singlet for Fe(II) complexes, doublet for Fe(III) complexes and triplet for Fe(IV) complexes) to be more stable than the high-spin state in all cases, and hence overstabilizes the low-spin state irrespective of the ligand environment around the iron center. The most recently developed meta-NGA functional that we study here is MN15-L, has the same mathematical form as the earlier MN12-L functional,[147] but has been optimized with a larger database and smoothness constraints. The MN15-L functional predicts the correct spin state for only **8** complexes and heavily favors high spin states. Thus the NGA, namely GAM, is more suitable for studying spin crossover in iron complexes than the meta-NGA, namely MN15-L.

We also used the M06, PW6B95, SOGGA11-X, MPW1B95, MN15 and M08-SO functionals, which have kinetic energy density terms and a nonzero percentage of HF exchange. M08-SO gives correct predictions for only 6 out of 14 complexes owing to overstabilization of high-spin state, M06 and SOGGA11-X give correct predictions for 9 out of 14 complexes, and the more recent functional MN15 and MPW1B95 give correct predictions for 13 out of 14 complexes. The best performing functional is PW6B95, which correctly predicts the ground spin state of all 14 complexes.

To summarize this section, we have found that three local density functionals, namely OPBE, OLYP and M06-L, three hybrid GGAs, namely B3LYP*, B3LYP and PBE0, the hybrid meta-NGA, namely MN15, and two hybrid meta-GGAs, PW6B95 and MPW1B95, show good performance in the prediction of the ground spin states of the iron complexes. Note that OPBE, OLYP and M06-L have no HF exchange and are less expensive than hybrid functionals for calculations on very large systems.

4.1.4 Metal–ligand distances in different spin state complexes. For the metal complexes studied here, the different spin states affect the environment of the central atom and the metal–ligand distances. The average of all six metal–ligand distances (defined, *e.g.*, as the metal–carbon distances for CO ligands and as the metal–oxygen distances for water ligands), were calculated for PW6B95 optimized geometries of three spin states of two complexes – $[Fe(H_2O)_6]^{2+}$ and $[Fe(CO)_6]^{2+}$. The trend we found is the same as found previously,[48] namely that the high-spin states have longer metal–ligand distances than the low-spin ones. Furthermore, the strong field ligands introduce more significant changes for metal–ligand distances than the weak field ligands. As examples, Table 8 shows the average metal–ligand distances of $[Fe(H_2O)_6]^{2+}$ and $[Fe(CO)_6]^{2+}$ complexes for their quintet, triplet and singlet spin states, where the H_2O ligands are weak-field ligands and the CO ligands are strong-field ones. In the case of CO ligands the average bond length difference for singlet and quintet states is $\sim$0.4 Å, and this difference is decreased to $\sim$0.1 Å for H_2O ligands.

4.1.5 Molecular orbital (MO) diagrams of 3d spin–orbitals of Fe(II) complexes. In textbook discussions of spin ground states of octahedral complexes, one considers the splitting of a fivefold degenerate d orbital manifold into e orbitals and t orbitals by a crystal field or ligand field, with a large splitting by strong-field ligands favoring low-spin states and a small splitting by weak-field ligands favoring high-spin states.[148,149] However this picture does not mesh well with the description provided by KS-DFT. A basic aspect of KS-DFT is that the electron density is represented as the absolute square of a Slater determinant. As pointed out by Görling,[150] the Kohn–Sham Slater determinant cannot in general be assigned to an irreducible representation of the symmetry group of the system (in addition to the fact that it does not correspond to a definite value of total electron spin). This is not a failure of presently available exchange–correlation functionals but rather a feature of how conventional Kohn–Sham

Table 8 Average metal–ligand distances (in Å) of $[Fe(H_2O)_6]^{2+}$ and $[Fe(CO)_6]^{2+}$ complexes in their quintet, triplet, and singlet spin states as optimized by PW6B95/def2-TZVP

Complex	Quintet	Triplet	Singlet
$[Fe(H_2O)_6]^{2+}$	2.147	2.099	2.048
$[Fe(CO)_6]^{2+}$	2.310	2.128	1.938

theory works, as disconcerting as it might be for those who wish to use ideas ingrained from long usage of wave function theory.[151] Therefore, to understand why the different exchange–correlation functionals studied here lead to different predictions for the ground-state spin state, we must work with spatial orbitals that do not show the usually expected symmetries. For example, the Kohn–Sham Slater determinant of Fe^{2+} monatomic ion does not have fivefold degenerate d orbitals, and the splitting is a few eV, which is not insignificant. Furthermore (and this aspect is already familiar from unrestricted HF theory), the spatial orbitals and spin–orbital energies for majority spins (α spins) differ from those for minority spins (β spins). Therefore we must look at spin–orbital energies, not orbital energies, and we will do that.

To investigate the energy splitting of 3d spin–orbitals in the central Fe atom of complexes in different spin states, we selected for comparison a weak-field ligand complex, $[Fe(H_2O)_6]^{2+}$, and a strong-field one, $[Fe(CO)_6]^{2+}$. (In these cases we can identify the d orbitals reasonably clearly from plots of the orbital amplitude contours, but we note that in some other cases, for example $[Fe(bipy)_3]^{2+}$, the d orbitals show strong mixing with the ligand orbitals, which complicates the analysis further.) We chose two functionals: PW6B95, which predicts the energetic ground spin state correctly for all 14 complexes, and M11-L, which has poor performance for the prediction of which is the ground spin state.

Fig. 3 shows the α and β spin–orbital energies for all the occupied and unoccupied d orbitals; the degenerate and nearly degenerate energy levels are shown by multiple short lines, with the energy level terms shifted horizontally simply for visibility if terms are very close to each other. The gray dotted lines connect matching α and β spin–orbitals. Below the orbital diagrams are the relative total energies of the states (denoted ΔE) and also the sum of the spin–orbital energies of the occupied d orbitals (denoted by $\Delta\varepsilon$(d)).

In the top left plot of Fig. 3 the d spin–orbital energy levels of quintet, triplet and singlet spin states as calculated by PW6B95 are shown for $[Fe(CO)_6]^{2+}$. Since CO is a strong-field ligand, the ground spin state is singlet (see the ΔE values in the figure), and the singlet state shows the usual picture, namely three degenerate d orbitals that are doubly occupied, and two degenerate d orbitals that are empty. To make the triplet, we move a β electron from this state to an empty α orbital. The figure shows that this action breaks both three-fold degeneracies and both two-fold ones. To make the quintet, one promotes another β electron from this state to an empty α orbital, which now breaks one of the two remaining spin–orbital degeneracies; interestingly, the double degeneracy in the α manifold remains. In the plot only the d orbitals are shown, but we note that there are several π-type ligand orbitals with orbital energies around −21 eV, so the 3d subshell does not form a single contiguous block on a full spin–orbital diagram. Fig. 3 makes it clear that we must consider the changes in spin–orbital energies when the spin state changes, not just move electrons in a diagram with fixed spin–orbital energies or fixed orbital energies. The spin–orbital energies change in part because there are new favorable exchange interactions among the α orbitals when we increase M_S and fewer favorable interactions in the β manifold; and they also change because the geometry changes.

Furthermore, as complicated as the changes in spin–orbital energies are, they still do not present a complete picture. To illustrate this issue we approximated the difference in spin-state energies as the difference in the sum of the occupied spin–orbital energies of the d orbitals. This would give the correct spin-state energy differences if two conditions were fulfilled: (i) the total energies were equal to the sum of the spin–orbital energies and (ii) the spin–orbital energies of the other spin–orbitals did not change appreciably upon moving electrons between the α and β manifolds of d orbitals. Detailed examination of the calculations shows that neither of these conditions is even close to being satisfied, and indeed the figure shows that the sum of the d spin–orbital energies does not even predict the correct direction of the energy change upon a spin transition in the case of PW6B95 calculations on $[Fe(CO)_6]^{2+}$ or for M11-L calculations on $[Fe(H_2O)_6]^{2+}$, although it does give the correct signs of the energy differences for PW6B95 calculations on $[Fe(H_2O)_6]^{2+}$. Based on these considerations and on those in the previous paragraph, we conclude that the usual way of thinking about spin-state energetic trends in terms of weak-field and strong-field effects on d orbital energies is overly simplified.

If the two top MO diagrams, namely $[Fe(CO)_6]^{2+}$ by PW6B95 and M11-L, are compared, one sees that the patterns of energy levels are similar for singlet and quintet but not for triplet. Perhaps more significantly, one also sees that in the case of M11-L the range of d spin–orbital energies is compressed. In particular, with M11-L the energy differences between the lowest- and highest-energy occupied d spin–orbitals as well as between the highest-energy occupied and the lowest-energy unoccupied d spin–orbitals are about 2 eV smaller than those values by PW6B95. The same compression is noticeable if one compares the bottom left to the bottom right. Since the reason for the failing of the M11-L functional is that it always predicts the ground spin state to be the singlet (even when it should be a higher-spin state), the conventional argument would have led one to expect a greater spread of energies of the spin–orbitals for this functional. Thus orbital plots like this do not even have a shred of usefulness in explaining the spin state energetics or the trends among the functionals.

If we compare the two left-side MO diagrams, namely those for $[Fe(CO)_6]^{2+}$ and $[Fe(H_2O)_6]^{2+}$ by PW6B95, then the patterns of the energy levels are similar for all three spin states, but in the case of $[Fe(H_2O)_6]^{2+}$ the presence of orbital degeneracies is decreased compared to $[Fe(CO)_6]^{2+}$. Because of the smaller effect of the weak-field ligands (H_2O), the d orbitals are situated higher in energy then in the case of strong-field ligands (CO).

4.2 Spin–orbit coupling terms

Table 9 shows the computed spin–orbit coupling (SOC) values for nine iron complexes.

The Fe(II) quintet complexes were calculated using five equally weighted states because the maximum number of configuration state functions (CSFs) for six electrons distributed in five 3d orbitals with active space (6/5) is five.

The Fe(III) doublet complexes have 75 possible CSFs with the (5/5) active space, but the maximum number of states allowed by *Molpro* version 2010 is only 20 for each irreducible

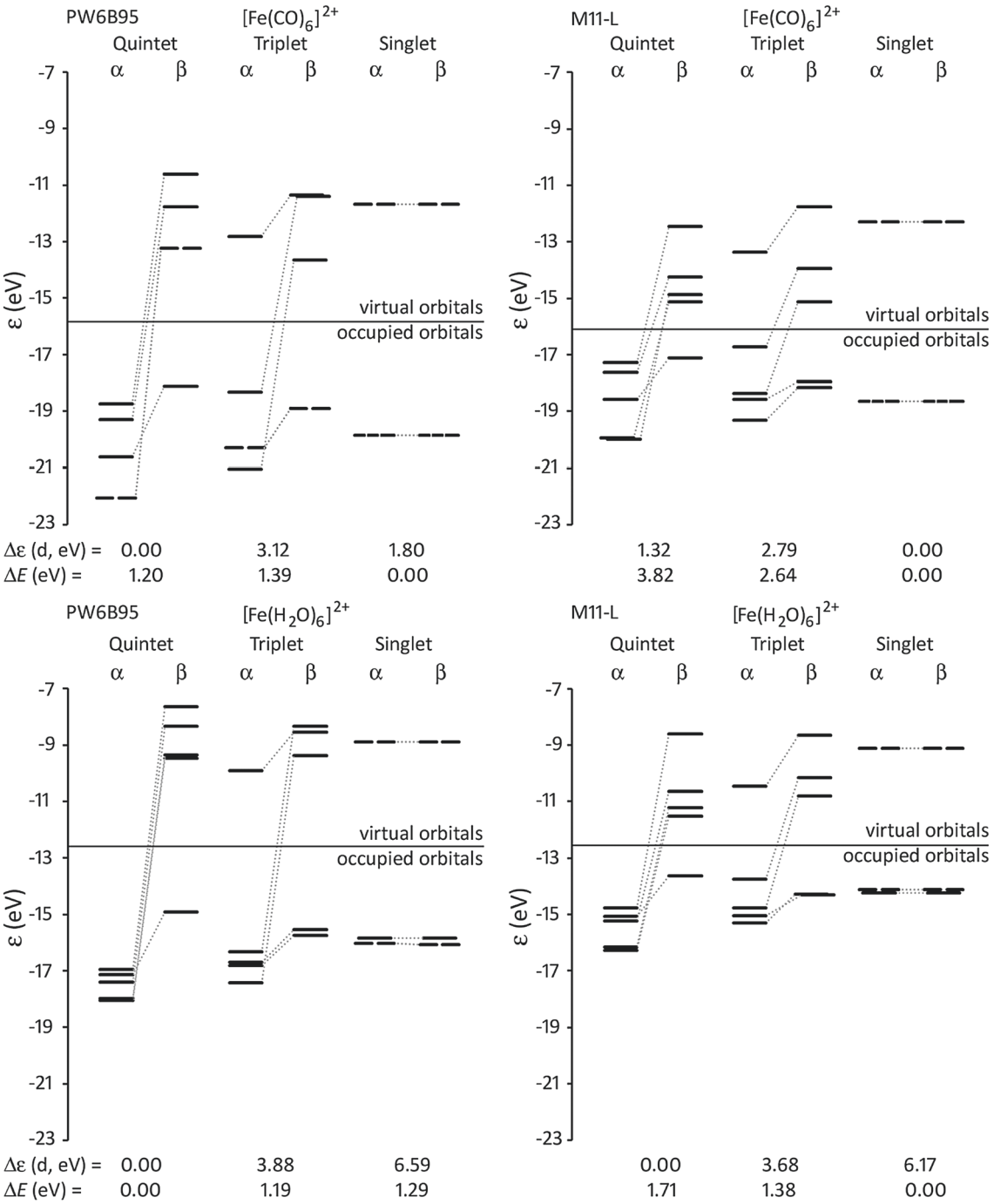

Fig. 3 MO diagrams of 3d orbitals for quintet, triplet and singlet spin states of two Fe(II) complexes calculated by the PW6B95 and M11-L exchange–correlation functionals; $\Delta\varepsilon$ (d, eV) and ΔE (eV) are the relative energy differences between the spin states calculated approximately using the sum of occupied 3d spin–orbital energies and calculated correctly using the total energies, respectively. (Note that ΔE and $\Delta\varepsilon$(d) each have their own zero of energy for relative energies.)

representation. Since we are not able to take into account all of the possible 75 configurations, it is important to consider the sensitivity of SOC to the number of states. Thus SOC effects were calculated using five states, 10 states, and 20 states. The five states and 20 states calculations gave a maximum difference of 0.3 kcal mol^{-1}. The results obtained with 10-state and 20-state calculations were very similar to each other, but since the 20-state calculations would be expected to be more accurate, we report 20-state calculations in Table 9. However, only the doublet state of the four Fe(III) complexes is reported with 20 states, while the remaining calculations in the table are based on using five states.

For all the studied complexes, we find that the magnitude of SOC is not more than 1.3 kcal mol^{-1}, and its effect on energy splitting is discussed in the next section.

Table 9 Spin–orbit coupling (SOC, kcal mol^{-1}) computed with CASSCF(6/5)/cc-pVDZ//GAM/def2-TZVP for Fe(II) complexes and CASSCF(5/5)/cc-pVDZ//GAM/def2-TZVP for Fe(III) complexes

Complex	E_{SOC}[a] (HS)	E_{SOC}[a] (LS)
Fe(II)[b]		
$[Fe(CO)_6]^{2+}$	−0.9	0.0
$[Fe(CNH)_6]^{2+}$	−0.9	0.0
$[Fe(NCH)_6]^{2+}$	−0.9	0.0
$[Fe(NH_3)_6]^{2+}$	−0.7	0.0
$[Fe(H_2O)_6]^{2+}$	−0.5	0.0
Fe(III)[c]		
$[Fe(CO)_6]^{3+}$	0.0	−0.6
$[Fe(CNH)_6]^{3+}$	0.0	−0.6
$[Fe(NCH)_6]^{3+}$	0.0	−1.3
$[Fe(NH_3)_6]^{3+}$	0.0	−1.3

[a] HS = high-spin; LS = low-spin. [b] For Fe(II) complexes, HS = quintet calculated with 5 states and LS = singlet. [c] For Fe(III) complexes, HS = sextet and LS = doublet calculated with 20 states.

4.3 Effect of spin–orbit coupling on calculated energy splitting

In this section, we examine the effect of spin–orbit coupling energies shown in Table 9, on the calculated energy splittings of nine complexes. These results are summarized in Table 10. Except for MN15, we find inclusion of the spin–orbit coupling does not change our conclusions about the number of correct predictions for the ground spin state by each functional. The conclusions do not change in most cases because the maximum contribution due to spin–orbit coupling in Table 9 does not exceed 1.3 kcal mol^{-1}, and this is quite small relative to most of the energy level differences reported in Tables 5 and 6. For $[Fe(NCH)_6]^{3+}$ with MN15, the energy splitting before including spin–orbit coupling was −0.6 kcal mol^{-1} and after inclusion it becomes 0.6 kcal mol^{-1}. The sign change changes the prediction of whether the high- or low-spin state is the ground state, but with such a small value of energy splitting between high- and low-spin states for this complex we can say that the two spin states are nearly degenerate according to this functional.

4.4 Effect of basis set and scalar relativity on calculated energy splittings

Some effects of basis set choice have been examined in previous work,[152,153] and here we examine them in the present context. In Table 11 we investigate the basis set size effect, the effect of core-valence correlation in basis sets and the effect of using the second-order Douglas–Kroll–Hess (DKH) method[154] to include scalar relativistic effects. We consider these effects for the $[Fe(NCH)_6]^{2+}$, $[Fe(O)(TMC)(MeCN)]^{2+}$ and $[Fe(O)(TMCS)]^{+}$ complexes. The detailed study of $[Fe(NCH)_6]^{2+}$ is motivated by the fact that the calculated spin splitting obtained at the M06-L/def2-TZVP level is small (1.9 kcal mol^{-1}) when spin–orbit coupling is included. Hence we analyzed this complex to see if the predicted ground spin state would change if a larger basis set were used, and if the results above are an artifact of the basis set. The two Fe(IV)–O complexes, $[Fe(O)(TMC)(MeCN)]^{2+}$ and $[Fe(O)(TMCS)]^{+}$, are also analyzed for the same reason – in these cases using functionals that give magnitudes of quintet-triplet splitting less than or equal to 3 kcal mol^{-1}.

Some rows of Table 11 correspond to geometry optimization with the same basis set as used for the final energy calculation, and for others, the geometry was optimized with the def2-TZVP basis set and single-point calculations done with other basis sets, as indicated in the table. Calculations that use "...-DK" basis sets in Table 11 were carried out with the Douglas–Kroll–Hess scalar relativistic Hamiltonian; other calculations are nonrelativistic. Basis sets beginning with "cc-pwCV..." contain core polarization basis functions to account for core-valence correlation. We use a shorthand that "cc-(pw)CV..." denotes using cc-pwCV... for Fe but using cc-pV... for other atoms.

$[Fe(NCH)_6]^{2+}$. The results summarized in Table 11 show that as we increase the basis set size from def2-TZVP to ma-TZVP, from def2-QZVP to ma-QZVP, or from def2-QZVPP to ma-QZVPP, the results do not change at all or only change by a negligible amount (0.2 kcal mol^{-1}). This shows that minimal augmentation of the basis sets from Ahlrichs and coworkers with diffuse s and p basis functions does not change the results for the $[Fe(NCH)_6]^{2+}$

Table 10 Calculated energy splittings ($E_{HS} - E_{LS}$, kcal mol^{-1})[a] after including spin–orbit coupling for nine iron complexes using selected exchange–correlation functionals

Complex	GAM	M06-L	B3LYP	B3LYP*	PBE0	M06	MN15-L	MN15	Ref.
Fe(II) complexes[b]									
$[Fe(CO)_6]^{2+}$	34.6	42.4	29.9	42.1	31.0	22.0	19.4	32.2	Singlet
$[Fe(CNH)_6]^{2+}$	47.4	52.6	43.4	55.3	44.9	35.2	31.1	46.9	Singlet
$[Fe(NCH)_6]^{2+}$	−20.9	1.9	−4.1	3.2	−9.5	−14.1	−25.3[d]	−5.2	Quintet
$[Fe(NH_3)_6]^{2+}$	−35.7	−11.4	−13.4	−8.7	−19.9	−23.6	−34.9	−15.0	Quintet
$[Fe(H_2O)_6]^{2+}$	−59.2	−31.0	−28.6	−26.7	−33.7	−45.6	−58.1	−37.1	Quintet
Fe(III) complexes[c]									
$[Fe(CO)_6]^{3+}$	2.8	9.3	14.9	23.1	11.7	−2.1	−19.9	25.2	Doublet
$[Fe(CNH)_6]^{3+}$	21.2	24.9	31.9	40.4	29.4	14.9	−2.3	43.2	Doublet
$[Fe(NCH)_6]^{3+}$	−32.6	−18.3	−6.7	−1.0	−13.4	−28.7	−52.2	0.6	Sextet
$[Fe(NH_3)_6]^{3+}$	−24.2	−9.8	−0.3	4.7	−7.5	−19.9	−39.8	7.5	Sextet
No. of correct predictions	9	8	9	7	9	8	7	7	

[a] HS = high-spin and LS = low-spin; a positive $E_{HS} - E_{LS}$ implies that LS is the ground spin state and a negative value implies HS is the ground spin state. [b] For Fe(II) complexes, HS = quintet and LS = singlet. [c] For Fe(III) complexes, HS = sextet and LS = doublet. [d] The most stable wave function could not be obtained.

Table 11 Calculated spin-state splitting energies (ΔE, kcal mol^{-1}) of $[Fe(NCH)_6]^{2+}$, $[Fe(O)(TMCS)]^{+}$, and $[Fe(O)(TMC)(MeCN)]^{2+}$ complexes using selected functionals with several basis sets. The spin–orbit coupling was included in calculating the spin-state splitting energies of $[Fe(NCH)_6]^{2+}$

Functional	Basis for single-point	Basis for geometry optimization	Complex ΔE $[Fe(NCH)_6]^{2+}$ $E_{quintet} - E_{singlet}$[a]	Reference ground spin state
M06-L	def2-TZVP	Same	1.9	Quintet
	ma-TZVP	Same	1.7	
	ma-TZVPP	Same	1.2	
	def2-QZVP	Same	0.15	
	ma-QZVP	Same	0.15	
	def2-QZVPP	Same	0.14	
	ma-QZVPP	Same	0.14	
	def2-QZVP	def2-TZVP	0.15	
	cc-pVTZ	def2-TZVP	1.3	
	cc-pVTZ-DK	def2-TZVP	4.1	
	cc-(pw)CVTZ-DK	def2-TZVP	3.9	
	cc-(pw)CVQZ-DK	def2-TZVP	2.9	

Functional	Basis for single-point	Basis for geometry optimization	Complex ΔE $[Fe(O)(TMCS)]^{+}$ $E_{quintet} - E_{triplet}$[b]	Reference ground spin state
OPBE	def2-TZVP	Same	−1.8	Triplet
	def2-QZVP	def2-TZVP	−2.2	
	cc-pVTZ	def2-TZVP	−1.8	
	cc-pVTZ-DK	def2-TZVP	−1.5	
	cc-(pw)CVTZ-DK	def2-TZVP	−1.5	
	cc-(pw)CVQZ-DK	def2-TZVP	−1.8	
M06-L	def2-TZVP	Same	−2.1	
	def2-QZVP	def2-TZVP	−2.6	
	cc-pVTZ	def2-TZVP	−2.1	
	cc-pVTZ-DK	def2-TZVP	−2.0	
	cc-(pw)CVTZ-DK	def2-TZVP	−2.1	
	cc-(pw)CVQZ-DK	def2-TZVP	−2.5	
B3LYP	def2-TZVP	Same	−1.0	
	def2-QZVP	def2-TZVP	−1.2	
	cc-pVTZ	def2-TZVP	−0.8	
	cc-pVTZ-DK	def2-TZVP	−0.5	
	cc-(pw)CVTZ-DK	def2-TZVP	−0.5	
	cc-(pw)CVQZ-DK	def2-TZVP	−0.6	
B3LYP*	def2-TZVP	Same	1.8	
	def2-QZVP	def2-TZVP	1.6	
	cc-pVTZ	def2-TZVP	2.0	
	cc-pVTZ-DK	def2-TZVP	2.2	
	cc-(pw)CVTZ-DK	def2-TZVP	2.3	
	cc-(pw)CVQZ-DK	def2-TZVP	2.2	
PW6B95	def2-TZVP	Same	0.4	
	def2-QZVP	def2-TZVP	0.4	
	cc-pVTZ	def2-TZVP	0.6	
	cc-pVTZ-DK	def2-TZVP	1.0	
	cc-(pw)CVTZ-DK	def2-TZVP	1.1	
	cc-(pw)CVQZ-DK	def2-TZVP	1.0	
MPW1B95	def2-TZVP	Same	−0.9	
	def2-QZVP	def2-TZVP	−1.0	
	cc-pVTZ	def2-TZVP	−0.7	
	cc-pVTZ-DK	def2-TZVP	−0.3	
	cc-(pw)CVTZ-DK	def2-TZVP	−0.3	
	cc-(pw)CVQZ-DK	def2-TZVP	−0.4	

Functional	Basis for single-point	Basis for geometry optimization	Complex ΔE $[Fe(O)(TMC)(MeCN)]^{2+}$ $E_{quintet} - E_{triplet}$[b]	Reference ground spin state
OPBE	def2-TZVP	Same	2.9	Triplet
	def2-QZVP	def2-TZVP	2.6	
	cc-pVTZ	def2-TZVP	3.0	
	cc-pVTZ-DK	def2-TZVP	3.1	
	cc-(pw)CVTZ-DK	def2-TZVP	3.1	
	cc-(pw)CVQZ-DK	def2-TZVP	2.8	
OLYP	def2-TZVP	Same	2.3	
	def2-QZVP	def2-TZVP	2.1	
	cc-pVTZ	def2-TZVP	2.5	
	cc-pVTZ-DK	def2-TZVP	2.5	
	cc-(pw)CVTZ-DK	def2-TZVP	2.5	

Table 11 (*continued*)

Functional	Basis for single-point	Basis for geometry optimization	Complex ΔE $[Fe(O)(TMC)(MeCN)]^{2+}$ $E_{quintet} - E_{triplet}$ [b]	Reference ground spin state
	cc-(pw)CVQZ-DK	def2-TZVP	2.3	
PBE0	def2-TZVP	Same	1.6	
	def2-QZVP	def2-TZVP	1.4	
	cc-pVTZ	def2-TZVP	1.7	
	cc-pVTZ-DK	def2-TZVP	1.9	
	cc-(pw)CVTZ-DK	def2-TZVP	1.9	
	cc-(pw)CVQZ-DK	def2-TZVP	1.8	
B97-3	def2-TZVP	Same	−0.3	
	def2-QZVP	def2-TZVP	−0.4	
	cc-pVTZ	def2-TZVP	−0.1	
	cc-pVTZ-DK	def2-TZVP	0.1	
	cc-(pw)CVTZ-DK	def2-TZVP	0.1	
	cc-(pw)CVQZ-DK	def2-TZVP	−0.1	

[a] A positive $E_{quintet} - E_{singlet}$ implies that singlet is the ground spin state. [b] A positive $E_{quintet} - E_{triplet}$ implies that triplet is the ground spin state.

complex. However, increasing the basis set size from any of the triple-ζ to any of the quadruple-ζ type basis set affects the energy splitting by at least 1.0 kcal mol^{-1}.

Table 11 compares cc-pVTZ calculations to cc-pVTZ-DK calculations to see the contributions of scalar relativistic effects. We find that the DKH calculation has an effect of 2.8 kcal mol^{-1}.

Comparing calculations with the cc-(pw)CVTZ-DK basis set to those with the cc-pVTZ-DK basis set show that core-valence correlation has a negligible effect (0.2 kcal mol^{-1}). With all the basis sets tested, the sign of $E_{quintet} - E_{singlet}$ is found to be positive and therefore the predicted ground spin state remains singlet.

[Fe(O)(TMC)(MeCN)]$^{2+}$. The basis set effect and the effect of scalar relativity are tested for $[Fe(O)(TMC)(MeCN)]^{2+}$ with OPBE, OLYP, PBE0 and B97-3. For this complex, the maximum effect of basis set with any functional is 0.5 kcal mol^{-1}. The sign of $E_{quintet} - E_{triplet}$ predicted by various basis sets remains positive for OPBE, OLYP and PBE0, but, with B97-3 some basis sets give a positive sign and some negative. Moreover with B97-3 all the $|E_{quintet} - E_{triplet}|$ values are less than 0.5 kcal mol^{-1} indicating that the two spin states are nearly degenerate.

[Fe(O)(TMCS)]$^{+}$. The effect of basis set and DKH calculations for the $[Fe(O)(TMCS)]^{+}$ complex is tested using six density functionals – OPBE, M06-L, B3LYP, B3LYP*, PW6B95 and MPW1B95. With all of these functionals, the maximum basis-set effect is 0.7 kcal mol^{-1}, and the sign of $E_{quintet} - E_{triplet}$ predicted by these functionals does not change. Also with some of the functionals the $E_{quintet} - E_{triplet}$ values are very small and the two spin states can be considered to be nearly degenerate.

4.5 MN15 *vs.* MN15//M06-L

The two functionals, MN15 and M06-L, correctly predict the ground spin state of most of the iron complexes. In view of MN15 being a hybrid functional, and therefore computationally more expensive than the local functional, M06-L, we did single-point calculations using MN15/def2-TZVP//M06-L/def2-TZVP to see if we get results similar to MN15/def2-TZVP or not. If the results turn out to be similar, MN15/def2-TZVP//M06-L/def2-TZVP would be preferred over MN15/def2-TZVP when cost is a consideration. The results using these two methods are summarized in Table 12 for the five largest complexes – **6**, **7** and **12–14** (see Fig. 2) used in this work. We see that the difference between optimizations using MN15/def2-TZVP and single-point calculations using MN15/def2-TZVP on the M06-L/def2-TZVP optimized geometries is not more than 0.8 kcal mol^{-1}. Because the results using the two methods are so similar, one can use MN15/def2-TZVP//M06-L/def2-TZVP instead of MN15/def2-TZVP if it is more convenient.

Table 12 Calculated spin-state splitting energies of complexes **6**, **7**, and **12–14** using MN15/def2-TZVP and MN15/def2-TZVP//M06-L/def2-TZVP

Complex	MN15/def2-TZVP	MN15/def2-TZVP//M06-L/def2-TZVP
$E_{quintet} - E_{singlet}$		
6	5.9	5.8
7	−13.5	−13.8
$E_{triplet} - E_{singlet}$		
6	9.1	8.9
7	−4.0	−4.2
$E_{sextet} - E_{doublet}$		
12	21.6	22.0
$E_{quartet} - E_{doublet}$		
12	12.1	12.9
$E_{quintet} - E_{triplet}$		
13	6.1	5.5
14	−0.8	−0.3

5 Concluding remarks

In this work, ground spin states of the Fe^{2+} ion, FeO and 14 hexacoordinate iron complexes were examined using gas-phase electronic structure calculations.

Both the Fe^{2+} ion and FeO are known to have a quintet ground spin state from experiments. From density functional theory calculations, we find that most of the functionals predict the correct ground spin state for this ion and molecule, although state-energy splittings are generally poor, with low-spin states overstabilized relative to states of higher spin.

For the 14 hexacoordinate iron complexes, the hybrid functionals were found to be better than local functionals. With the def2-TZVP basis set, PW6B95 was found to get all the 14 complexes right, and B3LYP, MPW1B95 and MN15 correctly predicted the ground spin state of 13 out of 14 complexes. For the one case that each functional got wrong, the error was reasonably small: 0.6 kcal mol^{-1} for MN15, 0.9 kcal mol^{-1} for MPW1B95 and 1.0 kcal mol^{-1} for B3LYP. The good performance of PW6B95 is not particularly surprising because PW6B95 was found to be the best functional (out of a large number studied) when averaged over 3d and 4d transition metal energetics, main-group atomization energies, and alkyl bond energies,[56] and it was also found to very robust in broad tests by Goerigk and Grimme.[155]

Among the local functionals, the best performing functionals were OPBE, OLYP and M06-L; each of these predict the correct ground spin state for 12 out of 14 complexes. We especially note that OPBE performs better than PBE, and OLYP performs better than BLYP. We could get the correct ground spin state of most of the complexes with functionals that have various percentages of HF exchange, in particular with percentages ranging from 0 to 44; this shows that the percentage of HF exchange is only one of the relevant parameters, and a given functional has to be considered in its entirety.

Because local functionals are less computationally demanding than hybrid functionals for large systems, we did single-point calculations using MN15 at geometries determined with one of the best performing local functionals, M06-L (MN15//M06-L calculation), and we found the results using MN15 optimizations very similar to MN15//M06-L, making the latter method an excellent choice for calculations on large iron-containing systems.

Because those functionals that we found to be most accurate for hexacoordinate complexes are very inaccurate for the bare Fe^{2+} ion, it is evident that iron–ligand interactions in the complexes substantially changes the electronic distribution about the iron center. Therefore, if one is to carry out reliable validations of density functionals for practical applications to large molecules, it is necessary to carry out these validations based on databases with complexes representative of those to be involved in applications, as we have done here.

Competing financial interest

The authors declare no competing financial interest.

Acknowledgements

The authors are grateful to Laura Gagliardi and Haoyu Yu for helpful discussions and to Sam Odoh for assistance with the manuscript. This work was supported in part by the US Department of Energy, Office of Basic Energy Sciences, Division of Chemical Sciences, Geosciences, and Biosciences, under award DE-FG02-12ER16362 and in part by the US National Science Foundation (CHE-1361773 to L. Q. and CHE-1361595 to C. J. C.). PV acknowledges the Richard D. Amelar and Arthur S. Lodge Fellowship. J. E. M. N. K. acknowledges a Feodor Lynen Research Fellowship from the Alexander von Humboldt Foundation.

References

1 F. Ogliaro, N. Harris, S. Cohen, M. Filatov, S. P. de Visser and S. Shaik, A Model "Rebound" Mechanism of Hydroxylation by Cytochrome P450: Stepwise and Effectively Concerted Pathways, and Their Reactivity Patterns, *J. Am. Chem. Soc.*, 2000, **122**, 8977–8989.
2 M. Swart and M. Costas, *Spin States in Biochemistry and Inorganic Chemistry: Influence on Structure and Reactivity*, John Wiley & Sons, Ltd, 2015.
3 M. Swart and M. Gruden, Spinning Around in Transition-Metal Chemistry, *Acc. Chem. Res.*, 2016, **49**, 2690–2697.
4 H. Hirao, D. Kumar, W. Thiel and S. Shaik, Two States and Two More in the Mechanisms of Hydroxylation and Epoxidation by Cytochrome P450, *J. Am. Chem. Soc.*, 2005, **127**, 13007–13018.
5 H. Hirao, D. Kumar, L. Que, Jr and S. Shaik, Two-State Reactivity in Alkane Hydroxylation by Non-Heme Iron–Oxo Complexes, *J. Am. Chem. Soc.*, 2006, **128**, 8590–8606.
6 S. Shaik, H. Hirao and D. Kumar, Reactivity of High-Valent Iron–Oxo Species in Enzymes and Synthetic Reagents: A Tale of Many States, *Acc. Chem. Res.*, 2007, **40**, 532–542.
7 I. Bauer and H.-J. Knölker, Iron Catalysis in Organic Synthesis, *Chem. Rev.*, 2015, **115**, 3170–3387.
8 C. Walsh, Enabling the Chemistry of Life, *Nature*, 2001, **409**, 226–231.
9 P. Verma, K. D. Vogiatzis, N. Planas, J. Borycz, D. J. Xiao, J. R. Long, L. Gagliardi and D. G. Truhlar, Mechanism of Oxidation of Ethane to Ethanol at Iron(IV)–Oxo Sites in Magnesium-Diluted Fe_2(dobdc), *J. Am. Chem. Soc.*, 2015, **137**, 5770–5781.
10 B. E. R. Snyder, P. Vanelderen, M. L. Bols, S. D. Hallaert, L. H. Böttger, L. Ungur, K. Pierloot, R. A. Schoonheydt, B. F. Sels and E. I. Solomon, The Active Site of Low-Temperature Methane Hydroxylation in Iron-Containing Zeolites, *Nature*, 2016, **536**, 317–321.
11 P. Mal, D. Schultz, K. Beyeh, K. Rissanen and J. R. Nitschke, An Unlockable-Relockable Iron Cage by Subcomponent Self-Assembly, *Angew. Chem., Int. Ed.*, 2008, **47**, 8297–8301.
12 W. Meng, J. K. Clegg, J. D. Thoburn and J. R. Nitschke, Controlling the Transmission of Stereochemical Information through Space in Terphenyl-Edged Fe_4L_6 Cages, *J. Am. Chem. Soc.*, 2011, **133**, 13652–13660.
13 T. K. Ronson, A. B. League, L. Gagliardi, C. J. Cramer and J. R. Nitschke, Pyrene-Edged $Fe^{II}_4L_6$ Cages Adaptively Reconfigure During Guest Binding, *J. Am. Chem. Soc.*, 2014, **136**, 15615–15624.
14 A. L. Feig and S. J. Lippard, Reactions of Non-Heme Iron(II) Centers with Dioxygen in Biology and Chemistry, *Chem. Rev.*, 1994, **94**, 759–805.
15 E. G. Kovaleva and J. D. Lipscomb, Versatility of Biological Non-heme Fe(II) Centers in Oxygen Activation Reactions, *Nat. Chem. Biol.*, 2008, **4**, 186–193.
16 A. Mukherjee, M. A. Cranswick, M. Chakrabarti, T. K. Paine, K. Fujisawa, E. Münck and L. Que, Jr., Oxygen Activation at Mononuclear Nonheme Iron Centers: A Superoxo Perspective, *Inorg. Chem.*, 2010, **49**, 3618–3628.

17 J. L. Pierre and M. Fontecave, Iron and Activated Oxygen Species in Biology: The Basic Chemistry, *BioMetals*, 1999, **12**, 195–199.
18 H. A. Goodwin, Spin Transitions in Six-Coordinate Iron(II) Complexes, *Coord. Chem. Rev.*, 1976, **18**, 293–325.
19 H. Toftlund, Spin Equilibria in Iron(II) Complexes, *Coord. Chem. Rev.*, 1989, **94**, 67–108.
20 P. Gütlich and A. Hauser, Thermal and Light-Induced Spin Crossover in Iron(II) Complexes, *Coord. Chem. Rev.*, 1990, **97**, 1–22.
21 J. Hohenberger, K. Ray and K. Meyer, The Biology and Chemistry of High-Valent Iron–Oxo and Iron–Nitrido Complexes, *Nat. Commun.*, 2012, **3**, 720.
22 W. Nam, Synthetic Mononuclear Nonheme Iron–Oxygen Intermediates, *Acc. Chem. Res.*, 2015, **48**, 2415–2423.
23 W. N. Oloo and L. Que, Jr., Bioinspired Nonheme Iron Catalysts for C–H and C═C Bond Oxidation: Insights into the Nature of the Metal-Based Oxidants, *Acc. Chem. Res.*, 2015, **48**, 2612–2621.
24 I. Prat, J. S. Mathieson, M. Güell, X. Ribas, J. M. Luis, L. Cronin and M. Costas, Observation of Fe(V)═O Using Variable-Temperature Mass Spectrometry and its Enzyme-Like C–H and C═C Oxidation Reactions, *Nat. Chem.*, 2011, **3**, 788–793.
25 D. Kumar, B. Karamzadeh, G. N. Sastry and S. P. de Visser, What Factors Influence the Rate Constant of Substrate Epoxidation by Compound I of Cytochrome P450 and Analogous Iron(IV)–Oxo Oxidants?, *J. Am. Chem. Soc.*, 2010, **132**, 7656–7667.
26 J. F. Berry, S. D. George and F. Neese, Electronic Structure and Spectroscopy of ''Superoxidized'' Iron Centers in Model Systems: Theoretical and Experimental Trends, *Phys. Chem. Chem. Phys.*, 2008, **10**, 4361–4374.
27 E. D. Bloch, L. J. Murray, W. L. Queen, S. Chavan, S. N. Maximoff, J. P. Bigi, R. Krishna, V. K. Peterson, F. Grandjean, G. J. Long, B. Smit, S. Bordiga, C. M. Brown and J. R. Long, Selective Binding of O_2 over N_2 in a Redox-Active Metal–Organic Framework with Open Iron(II) Coordination Sites, *J. Am. Chem. Soc.*, 2011, **133**, 14814–14822.
28 D. J. Xiao, E. D. Bloch, J. A. Mason, W. L. Queen, M. R. Hudson, N. Planas, J. Borycz, A. L. Dzubak, P. Verma, K. Lee, F. Bonino, V. Crocellà, J. Yano, S. Bordiga, D. G. Truhlar, L. Gagliardi, C. M. Brown and J. R. Long, Oxidation of Ethane to Ethanol by N_2O in a Metal-Organic Framework with Coordinatively-Unsaturated Iron(II) Sites, *Nat. Chem.*, 2014, **6**, 590–595.
29 L. Shi, T. Wang, H. Zhang, K. Chang, X. Meng, H. Liu and J. Ye, An Amine-Functionalized Iron(III) Metal–Organic Framework as Efficient Visible-Light Photocatalyst for Cr(VI) Reduction, *Adv. Sci.*, 2015, **2**, 1500006.
30 K. G. M. Laurier, F. Vermoortele, R. Ameloot, D. E. De Vos, J. Hofkens and M. B. J. Roeffaers, Iron(III)-Based Metal–Organic Frameworks As Visible Light Photocatalysts, *J. Am. Chem. Soc.*, 2013, **135**, 14488–14491.
31 P. P. Knops-Gerrits and W. A. Goddard III, Methane Partial Oxidation in Iron Zeolites: Theory versus Experiment, *J. Mol. Catal. A: Chem.*, 2001, **166**, 135–145.
32 S. H. Choi, B. R. Wood, J. A. Ryder and A. T. Bell, X-ray Absorption Fine Structure Characterization of the Local Structure of Fe in Fe–ZSM-5, *J. Phys. Chem. B*, 2003, **107**, 11843–11851.
33 S. H. Choi, B. R. Wood, A. T. Bell, M. T. Janicke and K. C. Ott, X-ray Absorption Fine Structure Analysis of the Local Environment of Fe in Fe/Al–MFI, *J. Phys. Chem. B*, 2004, **108**, 8970–8975.
34 D. Schröder, S. Shaik and H. Schwarz, Two-State Reactivity as a New Concept in Organometallic Chemistry, *Acc. Chem. Res.*, 2000, **33**, 139–145.
35 S. Shaik, An Anatomy of the Two-State Reactivity Concept: Personal Reminiscences in Memoriam of Detlef Schröder, *Int. J. Mass Spectrom.*, 2013, **354–355**, 5–14.
36 H. Paulsen, L. Duelund, H. Winkler, H. Toftlund and A. X. Trautwein, Free Energy of Spin-Crossover Complexes Calculated with Density Functional Methods, *Inorg. Chem.*, 2001, **40**, 2201–2203.
37 K. P. Kepp, Consistent Descriptions of Metal–Ligand Bonds and Spin-Crossover in Inorganic Chemistry, *Coord. Chem. Rev.*, 2013, **257**, 196–209.
38 E. I. Ioannidis and H. J. Kulik, Towards Quantifying the Role of Exact Exchange in Predictions of Transition Metal Complex Properties, *J. Chem. Phys.*, 2015, **143**, 034104.
39 A. Droghetti, D. Alfè and S. Sanvito, Assessment of Density Functional Theory for Iron(II) Molecules Across the Spin-crossover Transition, *J. Chem. Phys.*, 2012, **137**, 124303.
40 S. Zein, S. A. Borshch, P. Fleurat-Lessard, M. E. Casida and H. Chermette, Assessment of the Exchange-Correlation Functionals for the Physical Description of Spin Transition Phenomena by Density Functional Theory Methods: All the Same?, *J. Chem. Phys.*, 2007, **126**, 014105.
41 A. Fouqueau, M. E. Casida, L. M. L. Daku, A. Hauser and F. Neese, Comparison of Density Functionals for Energy and Structural Differences Between the High- $[^5T_{2g}:(t_{2g})^4(e_g)^2]$ and Low- $[^1A_{1g}:(t_{2g})^6(e_g)^0]$ Spin States of Iron(II) Coordination Compounds. II. More Functionals and the Hexaminoferrous Cation, $[Fe(NH_3)_6]^{2+}$, *J. Chem. Phys.*, 2005, **122**, 044110.
42 A. Fouqueau, S. Mer, M. E. Casida, L. M. L. Daku, A. Hauser, T. Mineva and F. Neese, Comparison of Density Functionals for Energy and Structural Differences Between the High- $[^5T_{2g}:(t_{2g})^4(e_g)^2]$ and Low- $[^1A_{1g}:(t_{2g})^6(e_g)^0]$ Spin States of the Hexaquoferrous Cation $[Fe(H_2O)_6]^{2+}$, *J. Chem. Phys.*, 2004, **120**, 9473–9486.
43 L. M. L. Daku, A. Vargas, A. Hauser, A. Fouqueau and M. E. Casida, Assessment of Density Functionals for the High-Spin/Low-Spin Energy Difference in the Low-Spin Iron(II) Tris(2,2′-bipyridine) Complex, *ChemPhysChem*, 2005, **6**, 1393–1410.
44 K. Pierloot and S. Vancoillie, Relative Energy of the High-($^5T_{2g}$) and Low-($^1A_{1g}$) Spin States of $[Fe(H_2O)_6]^{2+}$, $[Fe(NH_3)_6]^{2+}$, and $[Fe(bpy)_3]^{2+}$: CASPT2 *versus* Density Functional Theory, *J. Chem. Phys.*, 2006, **125**, 124303.
45 M. Swart, Accurate Spin-State Energies for Iron Complexes, *J. Chem. Theory Comput.*, 2008, **4**, 2057–2066.
46 S. P. de Visser, What Factors Influence the Ratio of CsH Hydroxylation versus CdC Epoxidation by a Nonheme

Cytochrome P450 Biomimetic?, *J. Am. Chem. Soc.*, 2006, **128**, 15809–15818.
47 K. P. Kepp, Theoretical Study of Spin Crossover in 30 Iron Complexes, *Inorg. Chem.*, 2016, **55**, 2717–2727.
48 D. N. Bowman and E. Jakubikova, Low-Spin versus High-Spin Ground State in Pseudo-Octahedral Iron Complexes, *Inorg. Chem.*, 2012, **51**, 6011–6019.
49 E. Ruiz, P. Alemany, S. Alvarez and J. Cano, Toward the Prediction of Magnetic Coupling in Molecular Systems: Hydroxo- and Alkoxo-Bridged Cu(II) Binuclear Complexes, *J. Am. Chem. Soc.*, 1997, **119**, 1297–1303.
50 J. Conradie and A. Ghosh, DFT Calculations on the Spin-Crossover Complex Fe(salen)(NO): A Quest for the Best Functional, *J. Phys. Chem. B*, 2007, **111**, 12621–12624.
51 C. J. Cramer and D. G. Truhlar, Density Functional Theory for Transition Metals and Transition Metal Chemistry, *Phys. Chem. Chem. Phys.*, 2009, **11**, 10757–10816.
52 M. Swart, Spin States of (Bio)inorganic Systems: Successes and Pitfalls, *Int. J. Quantum Chem.*, 2013, **113**, 2–7.
53 O. Gunnarsson and R. O. Jones, Total-Energy Differences: Sources of Error in Local-Density Approximations, *Phys. Rev. B: Condens. Matter Mater. Phys.*, 1985, **31**, 7588–7602.
54 K. R. Yang, R. Peverati, D. G. Truhlar and R. Valero, Density Functional Study of Multiplicity-Changing Valence and Rydberg Excitations of p-Block Elements: ΔSCF, Collinear Spin-Flip Time-Dependent DFT, and Conventional Time-Dependent DFT, *J. Chem. Phys.*, 2011, **135**, 044118.
55 S. Luo and D. G. Truhlar, How Evenly Can Approximate Density Functionals Treat the Different Multiplicities and Ionization States of 4d Transition Metal Atoms?, *J. Chem. Theory Comput.*, 2012, **8**, 4112–4126.
56 S. Luo, B. Averkiev, K. R. Yang, X. Xu and D. G. Truhlar, Density Functional Theory of Open-Shell Systems. The 3d-Series Transition Metal Atoms and Their Cations, *J. Chem. Theory Comput.*, 2014, **10**, 102–121.
57 T. Schmidt and S. Kümmel, One- and Many-Electron Self-Interaction Error in Local and Global Hybrid Functionals, *Phys. Rev. B: Condens. Matter Mater. Phys.*, 2016, **93**, 165120.
58 M. Reiher, O. Salomon and B. A. Hess, Reparameterization of Hybrid Functionals Based on Energy Differences of States of Different Multiplicity, *Theor. Chem. Acc.*, 2001, **107**, 48–55.
59 O. Salomon, M. Reiher and B. A. Hess, Assertion and Validation of the Performance of the B3LYP* Functional for the First Transition Metal Row and the G2 Test Set, *J. Chem. Phys.*, 2002, **117**, 4729–4737.
60 G. Ganzenmüller, N. Berkaïne, A. Fouqueau, M. E. Casida and M. Reiher, Comparison of Density Functionals for Differences Between the High- ($^5T_{2g}$) and low- ($^1A_{1g}$) Spin States of Iron(ii) Compounds. IV. Results for the Ferrous Complexes [Fe(*L*)('NHS_4')], *J. Chem. Phys.*, 2005, **122**, 234321.
61 M. Bruschi, L. De Gioia, G. Zampella, M. Reiher, P. Fantucci and M. Stein, A Theoretical Study of Spin States in Ni–S4 Complexes and Models of the [NiFe] Hydrogenase Active Site, *J. Biol. Inorg. Chem.*, 2004, **9**, 873–884.
62 D. M. A. Smith, M. Dupuis and T. P. Straatsma, Multiplet Splittings and Other Properties from Density Functional Theory: An Assessment in Iron-Porphyrin Systems, *Mol. Phys.*, 2005, **103**, 273–278.
63 M. Swart, A. R. Groenhof, A. W. Ehlers and K. Lammertsma, Validation of Exchange–Correlation Functionals for Spin States of Iron Complexes, *J. Phys. Chem. A*, 2004, **108**, 5479–5483.
64 K. Pierloot and S. Vancoillie, Relative Energy of the High-($^5T_{2g}$) and Low-($^1A_{1g}$) Spin States of the Ferrous Complexes [Fe(*L*)(NHS_4)]: CASPT2 *versus* Density Functional Theory, *J. Chem. Phys.*, 2008, **128**, 034104.
65 W. C. Isley, III, S. Zarra, R. K. Carlson, R. A. Bilbeisi, T. K. Ronson, J. R. Nitschke, L. Gagliardi and C. J. Cramer, Predicting Paramagnetic ^{1}H NMR Chemical Shifts and State-Energy Separations in Spin-Crossover Host-Guest Systems, *Phys. Chem. Chem. Phys.*, 2014, **16**, 10620–10628.
66 N. C. Handy and A. J. Cohen, Left–Right Correlation Energy, *Mol. Phys.*, 2001, **99**, 403–412.
67 J. P. Perdew, K. Burke and M. Ernzerhof, Generalized Gradient Approximation Made Simple, *Phys. Rev. Lett.*, 1996, **77**, 3865–3868.
68 C. Lee, W. Yang and R. G. Parr, Development of the Colle-Salvetti Correlation-Energy Formula into a Functional of the Electron Density, *Phys. Rev. B: Condens. Matter Mater. Phys.*, 1988, **37**, 785–789.
69 B. Hammer, L. Hansen and J. Norskov, Improved Adsorption Energetics Within Density Functional Theory Using Revised Perdew–Burke–Ernzerhof Functionals, *Phys. Rev. B: Condens. Matter Mater. Phys.*, 1999, **59**, 7413–7421.
70 K. P. Jensen, B. O. Roos and U. Ryde, Performance of Density Functionals for First Row Transition Metal Systems, *J. Chem. Phys.*, 2007, **126**, 014103.
71 S. Grimme, Semiempirical Hybrid Density Functional with Perturbative Second-Order Correlation, *J. Chem. Phys.*, 2006, **124**, 034108.
72 N. E. Schultz, Y. Zhao and D. G. Truhlar, Density Functionals for Inorganometallic and Organometallic Chemistry, *J. Phys. Chem. A*, 2005, **109**, 11127–11143.
73 M. Radoń, Revisiting the Role of Exact Exchange in DFT Spin-State Energetics of Transition Metal Complexes, *Phys. Chem. Chem. Phys.*, 2014, **16**, 14479–14488.
74 W. M. C. Foulkes, L. Mitas, R. J. Needs and G. Rajagopal, Quantum Monte Carlo Simulations of Solids, *Rev. Mod. Phys.*, 2001, **73**, 33–83.
75 R. J. Needs, M. D. Towler, N. D. Drummond and P. López Ríos, Continuum Variational and Diffusion Quantum Monte Carlo Calculations, *J. Phys.: Condens. Matter*, 2010, **22**, 023201.
76 K. Andersson, P.-Å. Malmqvist and B. O. Roos, Second-Order Perturbation Theory with a Complete Active Space Self-Consistent Field Reference Function, *J. Chem. Phys.*, 1992, **96**, 1218–1226.
77 G. Ghigo, B. O. Roos and P.-Å. Malmqvist, *Chem. Phys. Lett.*, 2004, **396**, 142–149.
78 S. Sharma and G. K.-L. Chan, Spin-adapted density matrix renormalization group algorithms for quantum chemistry, *J. Chem. Phys.*, 2012, **136**, 124121.
79 J. L. Bao, S. O. Odoh, L. Gagliardi and D. G. Truhlar, Predicting Bond Dissociation Energies of Transition Metal

Compounds by Multiconfiguration Pair-Density Functional Theory and Second-Order Perturbation Theory Based on Correlated Participating Orbitals and Separated Pairs, *J. Chem. Theory Comput.*, 2017, **13**, 616–626.

80 L. Wilbraham, P. Verma, D. G. Truhlar, L. Gagliardi and I. Ciofini, Multiconfiguration Pair-Density Functional Theory Predicts Spin-State Ordering in Iron Complexes with the Same Accuracy as Complete Active Space Second-Order Perturbation Theory at a Significantly Reduced Computational Cost, *J. Phys. Chem. Lett.*, 2017, **8**, 2026–2030.

81 A. D. Becke, Density-Functional Exchange-Energy Approximation with Correct Asymptotic Behavior, *Phys. Rev. A: At., Mol., Opt. Phys.*, 1988, **38**, 3098–3100.

82 J. P. Perdew, Density-Functional Approximation for the Correlation Energy of the Inhomogeneous Electron Gas, *Phys. Rev. B: Condens. Matter Mater. Phys.*, 1986, **33**, 8822–8824.

83 A. D. Becke, Density-Functional Thermochemistry. III. The Role of Exact Exchange, *J. Chem. Phys.*, 1993, **98**, 5648–5652.

84 S. Vancoillie, H. Zhao, M. Radoń and K. Pierloot, Performance of CASPT2 and DFT for Relative Spin-State Energetics of Heme Models, *J. Chem. Theory Comput.*, 2010, **6**, 576–582.

85 J.-U. Rohde, J.-H. In, M. H. Lim, W. W. Brennessel, M. R. Bukowski, A. Stubna, E. Münck, W. Nam and L. Que, Jr., Crystallographic and Spectroscopic Characterization of a Nonheme Fe(IV)=O Complex, *Science*, 2003, **299**, 1037–1039.

86 A. Thibon, J. England, M. Martinho, V. G. Young, Jr., J. R. Frisch, R. Guillot, J.-J. Girerd, E. Münck, L. Que, Jr. and F. Banse, Proton- and Reductant-Assisted Dioxygen Activation by a Nonheme Iron(II) Complex to Form an Oxoiron(IV) Intermediate, *Angew. Chem., Int. Ed.*, 2008, **47**, 7064–7067.

87 J. England, J. O. Bigelow, K. M. Van Heuvelen, E. R. Farquhar, M. Martinho, K. K. Meier, J. R. Frisch, E. Münck and L. Que, Jr., An Ultra-Stable Oxoiron(IV) Complex and its Blue Conjugate Base, *Chem. Sci.*, 2014, **5**, 1204–1215.

88 M. J. Frisch, G. W. Trucks, H. B. Schlegel, G. E. Scuseria, M. A. Robb, J. R. Cheeseman, G. Scalmani, V. Barone, B. Mennucci, G. A. Petersson, H. Nakatsuji, M. Caricato, X. Li, H. P. Hratchian, A. F. Izmaylov, J. Bloino, G. Zheng, J. L. Sonnenberg, M. Hada, M. Ehara, K. Toyota, R. Fukuda, J. Hasegawa, M. Ishida, T. Nakajima, Y. Honda, O. Kitao, H. Nakai, T. Vreven, J. A. Montgomery, Jr., J. E. Peralta, F. Ogliaro, M. Bearpark, J. J. Heyd, E. Brothers, K. N. Kudin, V. N. Staroverov, T. Keith, R. Kobayashi, J. Normand, K. Raghavachari, A. Rendell, J. C. Burant, S. S. Iyengar, J. Tomasi, M. Cossi, N. Rega, J. M. Millam, M. Klene, J. E. Knox, J. B. Cross, V. Bakken, C. Adamo, J. Jaramillo, R. Gomperts, R. E. Stratmann, O. Yazyev, A. J. Austin, R. Cammi, C. Pomelli, J. W. Ochterski, R. L. Martin, K. Morokuma, V. G. Zakrzewski, G. A. Voth, P. Salvador, J. J. Dannenberg, S. Dapprich, A. D. Daniels, O. Farkas, J. B. Foresman, J. V. Ortiz, J. Cioslowski and D. J. Fox, *Gaussian 09, Revision C.01*, Gaussian, Inc., Wallingford CT, 2010.

89 M. J. Frisch, G. W. Trucks, H. B. Schlegel, G. E. Scuseria, M. A. Robb, J. R. Cheeseman, G. Scalmani, V. Barone, B. Mennucci, G. A. Petersson, H. Nakatsuji, M. Caricato, X. Li, H. P. Hratchian, A. F. Izmaylov, J. Bloino, G. Zheng, J. L. Sonnenberg, M. Hada, M. Ehara, K. Toyota, R. Fukuda, J. Hasegawa, M. Ishida, T. Nakajima, Y. Honda, O. Kitao, H. Nakai, T. Vreven, J. A. Montgomery, Jr., J. E. Peralta, F. Ogliaro, M. Bearpark, J. J. Heyd, E. Brothers, K. N. Kudin, V. N. Staroverov, T. Keith, R. Kobayashi, J. Normand, K. Raghavachari, A. Rendell, J. C. Burant, S. S. Iyengar, J. Tomasi, M. Cossi, N. Rega, J. M. Millam, M. Klene, J. E. Knox, J. B. Cross, V. Bakken, C. Adamo, J. Jaramillo, R. Gomperts, R. E. Stratmann, O. Yazyev, A. J. Austin, R. Cammi, C. Pomelli, J. W. Ochterski, R. L. Martin, K. Morokuma, V. G. Zakrzewski, G. A. Voth, P. Salvador, J. J. Dannenberg, S. Dapprich, A. D. Daniels, O. Farkas, J. B. Foresman, J. V. Ortiz, J. Cioslowski and D. J. Fox, *Gaussian 09, Revision D.01*, Gaussian, Inc., Wallingford CT, 2013.

90 Y. Zhao, R. Peverati, S. Luo, K. R. Yang, X. He, H. S. Yu and D. G. Truhlar, *MN-GFM*, version 6.7: Minnesota–Gaussian Functional Module, http://comp.chem.umn.edu/mn-gfm.

91 W. Kohn and L. J. Sham, Self-Consistent Equations Including Exchange and Correlation Effects, *Phys. Rev.*, 1965, **140**, A1133–A1138.

92 R. Gáspár, Uber eine Approximation des Hartree-Fockschen Potentials durch eine universelle Potential Function, *Acta Phys. Hung.*, 1954, **3**, 263–286.

93 R. Gáspár, Statistical Exchange for Electron in Shell and the Xα Method, *Acta Phys. Hung.*, 1974, **35**, 213–218.

94 S. H. Vosko, L. Wilk and M. Nusair, Accurate Spin-Dependent Electron Liquid Correlation Energies for Local Spin Density Calculations: A Critical Analysis, *Can. J. Phys.*, 1980, **58**, 1200–1211.

95 R. Peverati and D. G. Truhlar, Exchange–Correlation Functional with Good Accuracy for Both Structural and Energetic Properties While Depending Only on the Density and its Gradient, *J. Chem. Theory Comput.*, 2012, **8**, 2310–2319.

96 H. S. Yu, W. Zhang, P. Verma, X. He and D. G. Truhlar, Nonseparable Exchange–Correlation Functional for Molecules, Including Homogeneous Catalysis Involving Transition Metals, *Phys. Chem. Chem. Phys.*, 2015, **17**, 12146–12160.

97 Y. Zhao and D. G. Truhlar, A New Local Functional for Main-Group Thermochemistry, Transition Metal Bonding, Thermodynamical Kinetics, and Non Covalent Interactions, *J. Chem. Phys.*, 2006, **125**, 194101.

98 R. Peverati and D. G. Truhlar, M11-L: A Local Density Functional That Provides Improved Accuracy for Electronic Structure Calculations in Chemistry and Physics, *J. Phys. Chem. Lett.*, 2012, **3**, 117–124.

99 H. S. Yu, X. He and D. G. Truhlar, MN15-L: A New Local Exchange-Correlation Functional for Kohn–Sham Density Functional Theory with Broad Accuracy for Atoms, Molecules, and Solids, *J. Chem. Theory Comput.*, 2016, **12**, 1280–1293.

100 P. Stephens, F. J. Devlin, C. F. Chabalowski and M. J. Frisch, Ab Initio Calculation of Vibrational Absorption and Circular Dichroism Spectra Using Density Functional Force Fields, *J. Phys. Chem.*, 1994, **98**, 11623–11627.

101 C. Adamo and V. Barone, Toward Reliable Density Functional Methods Without Adjustable Parameters: The PBE0 Model, *J. Chem. Phys.*, 1999, **110**, 6158–6170.

102 R. Peverati and D. G. Truhlar, Communication: A Global Hybrid Generalized Gradient Approximation to the Exchange-Correlation Functional that Satisfies the Second-Order Density-Gradient Constraint and has Broad Applicability in Chemistry, *J. Chem. Phys.*, 2011, **135**, 191102.

103 Y. Zhao and D. G. Truhlar, The M06 Suite of Density Functionals for Main Group Thermochemistry, Thermochemical Kinetics, Noncovalent Interactions, Excited States, and Transition Elements: Two New Functionals and Systematic Testing of Four M06-Class Functionals and 12 Other Functionals, *Theor. Chem. Acc.*, 2008, **120**, 215–241.

104 H. S. Yu, X. He, S. L. Li and D. G. Truhlar, MN15: A Kohn–Sham Global-Hybrid Exchange–Correlation Density Functional with Broad Accuracy for Multi-Reference and Single-Reference Systems and Noncovalent Interactions, *Chem. Sci.*, 2016, **7**, 5032–5051.

105 Y. Zhao and D. G. Truhlar, Hybrid Meta Density Functional Theory Methods for Thermochemistry, Thermochemical Kinetics, and Noncovalent Interactions: The MPW1B95 and MPWB1K Models and Comparative Assessments for Hydrogen Bonding and van der Waals Interactions, *J. Phys. Chem. A*, 2004, **108**, 6908–6918.

106 T. W. Keal and D. J. Tozer, Semiempirical Hybrid Functional with Improved Performance in an Extensive Chemical Assessment, *J. Chem. Phys.*, 2005, **123**, 121103.

107 Y. Zhao and D. G. Truhlar, Design of Density Functionals that are Broadly Accurate for Thermochemistry, Thermochemical Kinetics, and Nonbonded Interactions, *J. Phys. Chem. A*, 2005, **109**, 5656–5667.

108 Y. Zhao and D. G. Truhlar, Exploring the Limit of Accuracy of the Global Hybrid Meta Density Functional for Main-Group Thermochemistry, Kinetics, and Noncovalent Interactions, *J. Chem. Theory Comput.*, 2008, **4**, 1849–1868.

109 F. Weigend and R. Ahlrichs, Balanced Basis Set of Split Valence, Triple Zeta and Quadruple Zeta Valence Quality for H to Rn: Design and Assessment of Accuracy, *Phys. Chem. Chem. Phys.*, 2005, **7**, 3297–3305.

110 J. Zheng, X. Xu and D. G. Truhlar, Minimally Augmented Karlsruhe Basis Sets, *Theor. Chem. Acc.*, 2011, **128**, 295–305.

111 N. B. Balabanov and K. A. Peterson, Basis Set Limit Electronic Excitation Energies, Ionization Potentials, and Electron Affinities for the 3d Transition Metal Atoms: Coupled Cluster and Multireference Methods, *J. Chem. Phys.*, 2006, **125**, 074110.

112 N. B. Balabanov and K. A. Peterson, Systematically Convergent Basis Sets for Transition Metals. I. All-electron Correlation Consistent Basis Sets for the 3d Elements Sc-Zn, *J. Chem. Phys.*, 2005, **123**, 064107.

113 I. Ciofini and C. A. Daul, DFT Calculations of Molecular Magnetic Properties of Coordination Compounds, *Coord. Chem. Rev.*, 2003, **238**, 187–209.

114 F. Neese, Prediction of Molecular Properties and Molecular Spectroscopy with Density Functional Theory: From fundamental Theory to Exchange-Coupling, *Coord. Chem. Rev.*, 2009, **253**, 526–563.

115 H.-J. Werner, P. J. Knowles, G. Knizia, F. R. Manby, M. Schütz, P. Celani, T. Korona, R. Lindh, A. Mitrushenkov, G. Rauhut, K. R. Shamasundar, T. B. Adler, R. D. Amos, A. Bernhardsson, A. Berning, D. L. Cooper, M. J. O. Deegan, A. J. Dobbyn, F. Eckert, E. Goll, C. Hampel, A. Hesselmann, G. Hetzer, T. Hrenar, G. Jansen, C. Köppl, Y. Liu, A. W. Lloyd, R. A. Mata, A. J. May, S. J. Mcnicholas, W. Meyer, M. E. Mura, A. Nicklass, D. P. O'Neill, P. Palmieri, K. Pflüger, R. Pitzer, M. Reiher, T. Shiozaki, H. Stoll, A. J. Stone, R. Tarroni, T. Thorsteinsson, M. Wang and A. Wolf, *Molpro*, version 2010.1, http://www.molpro.net.

116 A. Berning, M. Schweizer, H.-J. Werner, P. J. Knowles and P. Palmieri, Spin–orbit Matrix Elements for Internally Contracted Multireference Configuration Interaction Wavefunctions, *Mol. Phys.*, 2000, **98**, 1823–1833.

117 K. K. Docken and J. Hinze, LiH Potential Curves and Wavefunctions for $X\,^1\Sigma^+$, $A\,^1\Sigma^+$, $B\,^1\Pi$, $^3\Sigma^+$, and $^3\Pi$, *J. Chem. Phys.*, 1972, **57**, 4928–4936.

118 K. Ruedenberg, L. M. Cheung and S. T. Elbert, MCSCF Optimization Through Combined Use of Natural Orbitals and the Brillouin–Levy–Berthier Theorem, *Int. J. Quantum Chem.*, 1979, **16**, 1069–1101.

119 B. O. Roos, The Complete Active Space SCF Method in a Fock-Matrix-Based Super-CI Formulation, *Int. J. Quantum Chem., Symp.*, 1980, **14**, 175–189.

120 H.-J. Werner and W. A. Meyer, A Quadratically Convergent MCSCF Method for the Simultaneous Optimization of Several States, *J. Chem. Phys.*, 1981, **74**, 5794–5801.

121 K. Ruedenberg, M. W. Schmidt, M. M. Gilbert and S. T. Elbert, Are Atoms Intrinsic to Molecular Electronic Wavefunctions? I. The FORS Model, *Chem. Phys.*, 1982, **71**, 41–49.

122 H.-J. Werner and P. J. Knowles, A Second Order Multiconfiguration SCF Procedure with Optimum Convergence, *J. Chem. Phys.*, 1985, **82**, 5053–5061.

123 P. J. Knowles and H.-J. Werner, An Efficient Second-Order MC SCF Method for Long Configuration Expansions, *Chem. Phys. Lett.*, 1985, **115**, 259–267.

124 L. Gagliardi and B. O. Roos, The Electronic Spectrum of $Re_2Cl_8^{2-}$: A Theoretical Study, *Inorg. Chem.*, 2003, **42**, 1599–1603.

125 L. Gagliardi, M. C. Heaven, J. W. Krogh and B. O. Roos, The Electronic Spectrum of the UO_2 Molecule, *J. Am. Chem. Soc.*, 2005, **127**, 86–91.

126 B. O. Roos, P.-Å. Malmqvist and L. Gagliardi, Exploring the Actinide-Actinide Bond: Theoretical Studies of the Chemical Bond in Ac_2, Th_2, Pa_2, and U_2, *J. Am. Chem. Soc.*, 2006, **128**, 1700–1706.

127 T. H. Dunning, Jr., Gaussian Basis Sets for Use in Correlated Molecular Calculations. I. The Atoms Boron through Neon and Hydrogen, *J. Chem. Phys.*, 1989, **90**, 1007–1023.

128 C. Moore, *Atomic Energy Levels*, National Bureau of Standards, Washington, DC, 1952, vol. 2.

129 A. Malassa, H. Görls, A. Buchholz, W. Plass and M. Westerhausen, Pyridylmethylamines as Ligands in Iron Halide Complexes – Coordination Behaviour Depending on the Halide, the Denticity of the Amino Ligand and the Oxidation State of Iron, *Z. Anorg. Allg. Chem.*, 2006, **632**, 2355–2362.

130 K. Wieghardt, W. Schmidt, W. Herrmann and H.-J. Küppers, Redox Potentials of Bis(1,4,7-triazacyclononane) Complexes of Some First Transition Series Metals(II, III). Preparation of Bis(1,4,7-triazacyclononane)nickel(III) Perchlorate, *Inorg. Chem.*, 1983, **22**, 2953.

131 M. R. Bukowski, K. D. Koehntop, A. Stubna, E. L. Bominaar, J. A. Halfen, E. Münck, W. Nam and L. Que, Jr., A Non-Heme Fe(IV) Complex with a Thiolate Ligand Relevant to P450, *Science*, 2005, **310**, 1000–1002.

132 J.-U. Rohde, J.-H. In, M. H. Lim, W. W. Brennessel, M. R. Bukowski, A. Stubna, E. Münck, W. Nam and L. Que, Jr., Crystallographic and Spectroscopic Characterization of a Nonheme Fe(IV)=O Complex, *Science*, 2003, **299**, 1037–1039.

133 C. N. Sakellaris, E. Miliordos and A. Mavridis, First Principles Study of the Ground and Excited States of FeO, FeO^+, and FeO^-, *J. Chem. Phys.*, 2011, **134**, 234308.

134 A. S.-C. Cheung, N. Lee, A. M. Lyyra, A. J. Merer and A. W. Taylor, Spectroscopic Properties of the $^5\Delta_i$ Ground State of FeO, *J. Mol. Spectrosc.*, 1982, **95**, 213.

135 C. V. Sastri, J. Lee, K. Oh, Y. J. Lee, J. Lee, T. A. Jackson, K. Ray, H. Hirao, W. Shin, J. A. Halfen, J. Kim, L. Que, Jr., S. Shaik and W. Nam, Axial Ligand Tuning of a Nonheme Iron(IV)–Oxo Unit for Hydrogen Atom Abstraction, *Proc. Natl. Acad. Sci. U. S. A.*, 2007, **104**, 19181–19186.

136 H. Hirao, L. Que, Jr., W. Nam and S. Shaik, A Two-State Reactivity Rationale for Counterintuitive Axial Ligand Effects on the C–H Activation Reactivity of Nonheme FeIV=O Oxidants, *Chem. – Eur. J.*, 2008, **14**, 1740–1756.

137 D. Mandal, R. Ramanan, D. Usharani, D. Janardanan, B. Wang and S. Shaik, How Does Tunneling Contribute to Counterintuitive H-abstraction Reactivity of Nonheme Fe(IV)O Oxidants with Alkanes?, *J. Am. Chem. Soc.*, 2015, **137**, 722–733.

138 A. R. McDonald and L. Que, Jr., High-Valent Nonheme Iron-Oxo Complexes: Synthesis, Structure, and Spectroscopy, *Coord. Chem. Rev.*, 2013, **257**, 414–428.

139 J. E. M. N. Klein and L. Que, Jr., Biomimetic High-Valent Mononuclear Nonheme Iron–Oxo Chemistry, *Encyclopedia of Inorganic and Bioinorganic Chemistry (EIBC)*, John Wiley & Sons, Ltd, 2016, DOI: 10.1002/9781119951438.eibc2344.

140 S. Shaik, H. Chen and D. Janardanan, Exchange-Enhanced Reactivity in Bond Activation by Metal-oxo Enzymes and Synthetic Reagents, *Nat. Chem.*, 2011, **3**, 19–27.

141 H. Chen, W. Lai and S. Shaik, Exchange-Enhanced H-Abstraction Reactivity of High-Valent Nonheme Iron(IV)–Oxo from Coupled Cluster and Density Functional Theories, *J. Phys. Chem. Lett.*, 2010, **1**, 1533–1540.

142 M. Swart and A. Change, in the Oxidation State of Iron: Scandium is not Innocent, *Chem. Commun.*, 2013, **49**, 6650–6652.

143 W. Yi, L. Yuan, Y. Kun, H. Zhengwen, T. Jing, F. Xu, G. Hong and W. Yong, What factors influence the reactivity of C–H hydroxylation and C=C epoxidation by $[Fe^{IV}(L_{ax})$(1,4,8,11-tetramethyl-1,4,8,11-tetraazacyclotetradecane)$(O)]^{n+}$, *J. Biol. Inorg. Chem.*, 2015, **20**, 1123–1134.

144 A. J. Johansson, M. R. A. Blomberg and P. E. M. Siegbahn, Quantifying the Effects of the Self-Interaction Error in Density Functional Theory: When Do the Delocalized States Appear? II. Iron-Oxo Complexes and Closed-Shell Substrate Molecules, *J. Chem. Phys.*, 2008, **129**, 154301.

145 R. Valero, R. Costa, I. de P. R. Moreira, D. G. Truhlar and F. Illas, Performance of the M06 Family of Exchange-Correlation Functionals for Predicting Magnetic Coupling in Organic and Inorganic Molecules, *J. Chem. Phys.*, 2008, **128**, 114103.

146 A. D. Becke, Density-Functional Thermochemistry. IV. A New Dynamical Correlation Functional and Implications for Exact-Exchange Mixing, *J. Chem. Phys.*, 1996, **104**, 1040–1046.

147 R. Peverati and D. G. Truhlar, An Improved and Broadly Accurate Local Approximation to the Exchange–Correlation Density Functional: The MN12-L Functional for Electronic Structure Calculations in Chemistry and Physics, *Phys. Chem. Chem. Phys.*, 2012, **14**, 13171–13174.

148 A. Yamamoto, *Organotransition Metal Chemistry*, Wiley, New York, 1986.

149 R. H. Crabtree, *The Organometallic Chemistry of the Transition Metals*, Wiley, New York, 2nd edn, 1994.

150 A. Görling, Symmetry in Density-Functional Theory, *Phys. Rev. A: At., Mol., Opt. Phys.*, 1993, **47**, 2783–2799.

151 M. Reiher, On the Definition of Local Spin in Relativistic and Nonrelativistic Quantum Chemistry, *Faraday Discuss.*, 2007, **135**, 97–124.

152 M. Güell, J. M. Luis, M. Solà and M. Swart, Importance of the Basis Set for the Spin-State Energetics of Iron Complexes, *J. Phys. Chem. A*, 2008, **112**, 6384–6391.

153 M. Swart, M. Güell, J. M. Luis and M. Solà, Spin-State-Corrected Gaussian-Type Orbital Basis Sets, *J. Phys. Chem. A*, 2010, **114**, 7191–7197.

154 B. A. Hess, Relativistic Electronic-Structure Calculations Employing a 2-Component No-Pair Formalism with External-Field Projection Operators, *Phys. Rev. A: At., Mol., Opt. Phys.*, 1986, **33**, 3742–3748.

155 L. Goerigk and S. Grimme, A Thorough Benchmark Of Density Functional Methods For General Main Group Thermochemistry, Kinetics, And Noncovalent Interactions, *Phys. Chem. Chem. Phys.*, 2011, **13**, 6670.

156 M. D. Allen, L. M. Ziurys and J. M. Brown, The Millimeter-Wave Spectrum of FeO in its X $^5\Delta_i$ State ($v = 0$): A Study of All Five Spin Components, *Chem. Phys. Lett.*, 1996, **257**, 130–136.

157 T. C. Steimle, J. Gengler and P. J. Hodges, The Permanent Electric Dipole Moments of Iron Monoxide, FeO, *J. Chem. Phys.*, 2004, **121**, 12303.

158 G. Drechsler, U. Boesl, C. Bäßmann and E. W. Schlag, Mass Selected Anion-Zero Kinetic Energy Photoelectron Spectroscopy (Anion-ZEKE): Ground and Low Excited States of FeO, *J. Chem. Phys.*, 1997, **107**, 2284–2291.

159 S. M. Harris and R. F. Barrow, Observations on the Electronic Spectrum of Gaseous FeO, *J. Mol. Spectrosc.*, 1980, **84**, 334–341.

160 J. B. Kim, M. L. Weichman and D. M. Neumark, Low-Lying States of FeO and FeO^- by Slow Photoelectron Spectroscopy, *Mol. Phys.*, 2015, **113**, 2105–2114.